Lattice QCD at nonzero isospin chemical potential

William Detmold, Kostas Orginos, and Zhifeng Shi

Phys. Rev. D **86**, 054507 — Published 17 September 2012

DOI: 10.1103/PhysRevD.86.054507

JLAB-THY-12-1548

Lattice QCD at non-zero isospin chemical potential

William Detmold,[1,2] Kostas Orginos,[1,2] and Zhifeng Shi[1,2]

[1]*Department of Physics, The College of William & Mary, Williamsburg, VA 23187, USA*

[2]*Jefferson Lab, Newport News, VA 23606, USA*

Abstract

Quantum chromodynamics (QCD) at non-zero isospin chemical potential is studied in a canonical approach by analyzing systems of fixed isospin number density. To construct these systems, we develop a range of new algorithms for performing the factorially large numbers of Wick contractions required in multi-hadron systems. We then use these methods to study systems with the quantum numbers of up to 72 π^+'s on three ensembles of gauge configurations with spatial extents $L \sim$ 2.0, 2.5 and 3.0 fm, and light quark masses corresponding to a pion mass of 390 MeV. The ground state energies of these systems are extracted and the volume dependence of these energies is utilized to determine the two- and three- body interactions amongst π^+'s. The systems studied correspond to isospin densities of up to $\rho_I \sim 9$ fm^{-3} and probe isospin chemical potentials, μ_I, in the range $m_\pi \lesssim \mu_I \lesssim 4.5\ m_\pi$, allowing us to investigate aspects of the QCD phase diagram at low temperature and for varying isospin chemical potential. By studying the energy density of the system, we provide numerical evidence for the conjectured transition of the system to a Bose-Einstein condensed phase at $\mu_I \gtrsim m_\pi$.

I. INTRODUCTION

An important goal of nuclear physics is to study the interactions and properties of systems comprised of large number of hadrons. Nuclear physics is an emergent phenomenon of the Standard Model and as this goal requires an understanding of the strong interaction dynamics of multi-hadron systems, it necessitates lattice QCD calculations. In recent years, preliminary studies of three- and four- baryon systems have been undertaken [1, 2] and more investigations are underway. In addition, systems involving up to twelve $\pi^{\pm}$'s [3, 4] or twelve $K^{\pm}$'s [5] and systems comprised of more than one species [6] have been studied, allowing the various two- and three-body interaction parameters of these systems to be determined from the energy shift of N-meson system at finite density.

The study of systems comprised of large numbers of hadrons can provide vital insight into the structure of high density mater, which may exist in the interiors of neutron stars [7], and it is also interesting from a purely theoretical point of view to study the rich phase structure of QCD. For systems of high isopin density, ρ_I, and non-zero isospin chemical potentials, μ_I, as will be studied here, a complex phase structure has been conjectured [8]. When μ_I reaches the mass of one pion, pions can be produced out of the vacuum and a Bose-Einstein condensate (BEC) is expected to form. At asymptotically large μ_I, the system is known to be a BCS-like state and at an intermediate isospin chemical potential, a BEC/BCS transition is expected to occur. However, the exact locations and natures of these BEC and the BEC/BCS transitions are unknown and can only be determined by non-perturbative QCD calculations. QCD studies of systems with finite baryon density are hampered by the sign problem resulting from the non-positivity of the determinant of the Dirac operator. However for systems with non-zero isospin chemical potential, there is no sign problem. There have recently been interesting relationships found between large N theories with isopin and baryon chemical potentials [9–11], further motivating the study of systems at non-zero isospin chemical potential. By introducing an isospin chemical potential into the QCD action, non-zero isospin density systems have been studied in Ref. [12–14], showing hints of some aspects of the expected phase structure. Non-zero isospin density system can also be studied by the direct computation of correlation function of increasing numbers of pions [3–5] and the extension of these methods is the subject of the current work.

Calculating correlation functions involving many-meson systems (here we will focus on

many π^+ systems) involves computing all possible contractions between quark field operators, the number of which naively grows as $N!N!$ for mesonic systems. Even considering symmetries between up and down quarks and identifying vanishing and redundant contribution, the number of remaining contractions grows exponentially with N. In order to overcome this problem, much progress has been made in studying many meson systems in Ref. [15] by constructing a recursion relation for correlation functions of systems having different number of mesons, taking advantage of the fact that many contractions in the correlation function of an N-meson system have been partly computed for an $(N-1)$-meson system. Comparing with direct contractions, the recursion relation [15] saves tremendous amount of time, and systems having up to 24 π^+'s have been studied in [16] using it. Since the Pauli principle excludes putting more than $N_c N_s = 12$ quarks (where N_c and N_s are the number of color and spin components of the quark fields, respectively) in the same source location, additional sources are required for $N > 12$-meson[1] systems. In additional to requiring more quark propagators, this complicates the recursion relation and increases the computational cost of contractions such that the cost for $N = 24$ π^+'s is ~ 100 times that of 12 π^+'s. Studying systems of 36 π^+'s becomes extremely time consuming even with the recursion relation.

In the current work, we construct new methods to compute correlation function of systems containing large numbers of mesons of one species and also for muti-species systems by utilizing the fact that the ground state energy is independent of how the π^+'s are distributed among different source locations [16]. The new methods that are presented herein significantly speed up the contractions, and enable us to study even higher density systems, that are impractical with other methods. Using one of our new approaches, systems comprised of up to 72 π^+'s are studied on four ensembles of anisotropic clover lattices [17] with dimensions $16^3 \times 128$, $20^3 \times 128$, $24^3 \times 128$ and $20^3 \times 256$. This allows us to investigate multi-pion interactions and study the phase structure of QCD at non-zero μ_I. In this work, we are able to probe the QCD phase diagram from $\mu_I = m_\pi$ up to $\mu_I \approx 4.5\, m_\pi$. We provide strong evidence for the Bose-Einstein condensation of the system and attempt to investigate the BEC/BCS transition at larger μ_I.

[1] For simplicity we will refer to "N-meson" systems. More correctly, we deal with systems in which a conserved quantum number (such as isospin) is fixed to N.

The layout of this paper is as follows. In Section. II, we describe new methods to compute the correlation functions corresponding to many pion systems, and compare the performance and scalability of each method. Details of the lattice ensembles and our computation of the relevant correlation functions in momentum space are discussed in Section. III. By applying the most efficient contraction method, correlation function of systems comprised of up to 72 π^+'s are computed, and the ground state energies are extracted in Section. IV. In Section. V, the two-body and three-body interaction parameters are studied. In Section. VI, the QCD phase diagram at non-zero isospin chemical potential is investigated, and the transition to a BEC state is identified.

II. METHODOLOGY OF MULTI-MESON CONTRACTIONS

Non-zero isospin density meson systems can be studied by evaluating correlation functions of many π^+'s at finite volume (as we work in the context of a relativistic field theory, the pion number is ill-defined, however the net isospin of the system is specified in the correlation functions below). A correlation function for a system of $\overline{n} = \sum_{i=1}^{N} n_i$ π^+'s with n_i π^+'s from source locations $(\mathbf{y}_i, 0)$ is defined as:

$$C_{n_1,\ldots,n_N}(t) \;=\; \left\langle \left(\sum_{\mathbf{x}} \pi^+(\mathbf{x},t) \right)^{\overline{n}} \left(\pi^-(\mathbf{y_1},0) \right)^{n_1} \ldots \left(\pi^-(\mathbf{y_N},0) \right)^{n_N} \right\rangle , \qquad (1)$$

where the interpolating operator $\pi^+(\mathbf{x},t) = \overline{d}(\mathbf{x},t)\gamma_5 u(\mathbf{x},t)$ and $\pi^-(\mathbf{x},t) = \overline{u}(\mathbf{x},t)\gamma_5 d(\mathbf{x},t)$. According to Ref. [15], the correlator $C_{n_1,\ldots,n_N}$ can be identified as the term with prefactor $\prod_{i=1}^{N} \lambda_i^{n_i}$ from the expansion of $\det[1 + \lambda_1 P_1 + \lambda_2 P_2 + \ldots + \lambda_N P_N]$, where N is the number of sources, and the $12N \times 12N$ matrices P_k are given by:

$$P_k \;=\; \left(\begin{array}{c|ccc} 0 & 0 & 0 & 0 \\ \hline \vdots & \ldots & \ldots & \ldots \\ \hline P_{k,1} & P_{k,2} & \ldots & P_{k,N} \\ \hline \vdots & \ldots & \ldots & \ldots \\ \hline 0 & 0 & 0 & 0 \end{array} \right) , \qquad (2)$$

with 12×12 sub-blocks

$$P_{k,i}(t) = \sum_{\mathbf{x}} S(\mathbf{x},t;\mathbf{y}_i,0) S^\dagger(\mathbf{x},t;\mathbf{y}_k,0), \qquad (3)$$

where $S(\mathbf{x}, t; \mathbf{y}_i, 0)$ is a quark propagator between two points, and its γ_5 hermition property, $S(\mathbf{y}_k, t; \mathbf{x}, 0) = \gamma_5 S^\dagger(\mathbf{x}, t; \mathbf{y}_k, 0)\gamma_5$ has been used in the equation. Each $P_{k,i}$ is an uncontracted correlator describing a quark propagating from source i to source k through the sink at $\mathbf{x}$ with the quantum number of a π^+.

As shown in Ref. [15], a recursion relation for the $C_{n_1,..,n_N}(t)$ can be derived by studying the properties of the expansion of the above determinant. The $C_{n_1,...,n_N}(t)$'s have the same energy spectrum for all combinations of n_i's as long as $\overline{n}$ is fixed, so separately computing correlation functions of all possible combinations of n_i's is redundant. We can thus identify a combined correlator $C_{\overline{n}\pi}(t)$ as the term having prefactor λ^n from the expansion of $\det[1 + \lambda A]$, with

$$A = P_1 + P_2 + \ldots + P_N = \left(\begin{array}{c|c|c|c} P_{1,1} & P_{1,2} & \ldots & P_{1,N} \\ \hline \vdots & \ldots & \ldots & \ldots \\ \hline P_{k,1} & P_{k,2} & \ldots & P_{k,N} \\ \hline \vdots & \ldots & \ldots & \ldots \\ \hline P_{N,1} & P_{N,2} & \ldots & P_{N,N} \end{array}\right). \tag{4}$$

$C_{\overline{n}\pi}(t)$ is a complicated summation of all possible $C_{n_1,n_2,...,n_N}(t)$ with fixed $\overline{n}$, in which we do not identify which pions originate at which source. For multiple source contractions, even terms representing more than 12 π^+'s located in a single source are included, however such terms vanish identically and so do not produce additional noise in numerical calculations. As fewer correlation functions are needed, computing $C_{\overline{n}\pi}(t)$ is a computationally simpler task than recursively computing all $C_{n_1,n_2,...,n_N}(t)$. In the following subsections, we will construct four algorithms to further speed up the calculation of $C_{\bar{n}\pi}(t)$ and compare each algorithm in terms of precision requirement and numerical cost.

A. Vandermonde Matrix method (VMm)

As described above, a correlation function of an n-π^+ system ($C_{n\pi}$) can be identified as the coefficient of λ^n from the power series expansion of $\det[1 + \lambda A]$

$$\det[1 + \lambda A] = 1 + \lambda C_{1\pi} + \lambda^2 C_{2\pi} + \ldots + \lambda^{12N} C_{12N\pi}, \tag{5}$$

where A is a $12N \times 12N$ matrix constructed from uncontracted correlators following Eq. (4). A simple way to get $C_{n\pi}$ is by computing Eq. (5) for $12N$ different choices of λ ($\lambda_1, \ldots, \lambda_{12N}$).

The resulting system of equations can be written in the following matrix form

$$\begin{pmatrix} \frac{\det[1+\lambda_1 A]-1}{\lambda_1} \\ \frac{\det[1+\lambda_2 A]-1}{\lambda_2} \\ \vdots \\ \frac{\det[1+\lambda_{12N} A]-1}{\lambda_{12N}} \end{pmatrix} = \begin{pmatrix} 1 & \lambda_1 & \lambda_1^2 & \dots & \lambda_1^{12N-1} \\ 1 & \lambda_2 & \lambda_2^2 & \dots & \lambda_2^{12N-1} \\ \vdots & & & & \\ 1 & \lambda_n & \lambda_n^2 & \dots & \lambda_n^{12N-1} \end{pmatrix} \cdot \begin{pmatrix} C_{1\pi} \\ C_{2\pi} \\ \vdots \\ C_{12N\pi} \end{pmatrix}. \tag{6}$$

The matrix on the RHS of Eq. (6) is a $12N \times 12N$ Vandermonde matrix, for which there exist analytical forms for the determinant and inverse (see for example Ref. [18]). The inverse matrix then allows us to determine the $C_{n\pi}$'s from the numerical calculation of the determinant vector. However, when the number of sources becomes large, elements of this matrix can become very small or very large because of the factors of $\lambda_i^{1,2,\dots,12N-1}$, making the computation of the inverse very demanding in precision and eventually resulting in significant numerical errors.

B. FFT method (FFTm)

By choosing $\lambda = \exp(i2\pi f_0 \cdot \tau)$ in Eq. (5), the expansion becomes

$$\det[1 + \lambda A] = 1 + e^{2i\pi f_0 \cdot \tau} C_{1\pi} + e^{4i\pi f_0 \cdot \tau} C_{2\pi} + \ldots + e^{24i\pi N f_0 \cdot \tau} C_{12N\pi}, \tag{7}$$

which contains contributions from signals of frequencies kf_0, $k = 1, 2, \ldots 12N$. Because of this feature, the magnitude of each frequency component can easily be extracted using a Fast Fourier Transform (FFT). The magnitude corresponding to frequency kf_0 is equivalent to $C_{k\pi}$ times a normalization constant. In order to get better signals, data from multiple τ's are beneficial, which results in the need to calculate many determinants, in general making this method expensive. On the other hand, specific choices of f_0 and τ can minimize the number of required determinants. We set $\tau_n = n\ dt$, for $n = 1, 2, \ldots, T$ where dt is the minimal time step and T is the closest prime number larger than $12N$, and $f_0 = \frac{1}{dt \cdot T}$ and then compute $\det[1 + \lambda_n A]$ with $\lambda_n = \exp(i2\pi f_0 \cdot \tau_n)$. After applying the FFT to this series, the amplitude of the frequency kf_0 is $TC_{k\pi}$. With such choices of f_0, τ_n and T, the number of determinants needed to compute is the same as the Improved Combination method (ICm) discussed below.

C. Combination method (Cm)

The FFTm discussed above is constructed from a certain choice of λ's so that the expansion of the determinant can be recognized as contributions from different frequencies. Similarly, by studying the properties of Eq. (5), another choice of λ's can be utilized to eventually separate $\det[1+\lambda A]$ into groups of functions individually depending only on 3 correlation functions. This method requires us to determine the inverse of a 3×3 matrix, rather than a $12N\times 12N$ Vandermande matrix, to solve for the individual correlators. This method is applied by the following steps:

Step 1: Choose $f_1=1$ and compute

$$D_1^{(1)}(f_1\lambda)=\det[1+f_1\lambda A]-1. \tag{8}$$

Notice that $D_1^{(1)}(f_1\lambda)$ depends on all correlators $C_{1\pi},C_{2\pi},\ldots,C_{12N\pi}$.

Step 2: Choose $f_2=\exp(i\pi)$, and construct the following contractions of the functions $D_1^{(1)}(f_n\lambda)$ to generate the following two new quantities:

$$\begin{aligned} D_1^{(2)}(\lambda) &= D_1^{(1)}(f_1\lambda)+f_1D_1^{(1)}(f_2\lambda),\\ D_2^{(2)}(\lambda) &= D_1^{(1)}(f_1\lambda)+f_2D_1^{(1)}(f_2\lambda). \end{aligned} \tag{9}$$

By inserting the values of $f_1=1$, $f_2=-1$, it is clear that the $D_i^{(2)}(\lambda)$ only depend on $C_{(3-i)\pi},C_{(5-i)\pi},\ldots$, and so the correlation functions have been separated into two groups.

Step 3: Choose $f_3=\exp(i\frac{\pi}{2})$, and construct the following combinations of the functions $D_1^{(2)}(f_n\lambda)$ and $D_2^{(2)}(f_n\lambda)$:

$$\begin{aligned} D_1^{(3)}(\lambda) &= D_1^{(2)}(\lambda)+f_1D_1^{(2)}(f_3\lambda),\\ D_2^{(3)}(\lambda) &= D_1^{(2)}(\lambda)+f_2D_1^{(2)}(f_3\lambda),\\ D_3^{(3)}(\lambda) &= D_2^{(2)}(\lambda)+f_1f_3D_2^{(2)}(f_3\lambda),\\ D_4^{(3)}(\lambda) &= D_2^{(2)}(\lambda)+f_2f_3D_2^{(2)}(f_3\lambda), \end{aligned} \tag{10}$$

and we see that the $D_i^{(3)}(\lambda)$ for $i=1,2$ depends on $C_{(0+2i)\pi},C_{(4+2i)\pi},\ldots$, and $D_i^{(3)}(\lambda)$ for $i=3,4$ depends on $C_{(9-2i)\pi},C_{(13-2i)\pi},\ldots$. In each step, one function depending on a block of $C_{k\pi}$'s is separated into two functions each depending only on half of the $C_{k\pi}$'s from the previous function. We iterate this procedure until blocks of only 3 $C_{k\pi}$'s are reached.

To summarize this method, in "step n", $f_n = \exp(i\frac{\pi}{2^{n-2}})$ is chosen, and after this step $D_i^{(n-1)}(\lambda)$, $i = 1, \ldots, 2^{n-2}$, will be separated into 2^{n-1} functions, $D_i^{(n)}(\lambda)$, each depending on $12N/2^{n-1}$ $C_{k\pi}$'s. Assume $D_m^{(n-1)}(\lambda)$ is a function depending on a block of $C_{k\pi}$'s. Two functions, $D_{2m-1}^{(n)}$ and $D_{2m}^{(n)}$, each depending on a half of the original block of $C_{k\pi}$'s are constructed from $D_m^{(n-1)}(\lambda) + q_{2m-1} \cdot D_m^{(n-1)}(f_n \cdot \lambda)$ and $D_m^{(n-1)}(\lambda) + q_{2m} \cdot D_m^{(n-1)}(f_n \cdot \lambda)$, where the q_k's, $k = 1, 2, \ldots, 2^{n-1}$, are prefactors used to construct new functions depending only on half of the $C_{k\pi}$'s, which $D_m^{(n-1)}(\lambda)$ depends on. The prefactor q_k in step n is constructed in the following way.

$$
\begin{aligned}
&\text{Group 1:} && q_1 = f_1, \\
&\text{Group 2:} && q_2 = f_2 \cdot q_1, \\
&\text{Group 3:} && q_k = f_3 \cdot q_{k-2}, k = 3, 4, \\
& && \vdots \\
&\text{Group n:} && q_k = f_n \cdot q_{k-2^{n-2}}, k = 2^{n-2}+1, 2^{n-2}+2, ..., 2^{n-1},
\end{aligned} \tag{11}
$$

where "Group m" contains 2^{m-2} functions for $m = 2, 3, \ldots, n$. This process is repeated until functions, $D_k^{(\tilde{n})}(\lambda)$, each depending only on 3 $C_{i\pi}$'s are reached. Eventually $\det[1 + \lambda A]$ is separated into functions, $D_k^{(\tilde{n})}(\lambda)$, depending on following blocks (B_k):

$$
\begin{aligned}
&\text{Group 1:} && B_1 = [C_{4N\pi}, C_{8N\pi}, C_{12N\pi}] \\
&\text{Group 2:} && B_2 = [C_{2N\pi}, C_{6N\pi}, C_{10N\pi}] \equiv C_{\mathrm{Sub}(B_1)-2N} \\
&\text{Group 3:} && \begin{cases} B_3 = [C_{3N\pi}, C_{7N\pi}, C_{11N\pi}] \equiv C_{\mathrm{Sub}(B_1)-N} \\ B_4 = [C_{N\pi}, C_{5N\pi}, C_{9N\pi}] \equiv C_{\mathrm{Sub}(B_2)-N} \end{cases} \\
& \vdots \\
&\text{Group n:} && B_k = C_{\mathrm{Sub}(B_{k-2^{n-2}})-\frac{4N}{2^{n-2}}}, k = 2^{n-2}+1, 2^{n-2}+2, \ldots, 2^{n-1}
\end{aligned} \tag{12}
$$

where $\mathrm{Sub}(B_k)$ are the sub indexes of the C's in B_k, for example $\mathrm{Sub}(B_1) = \{4N, 8N, 12N\}$ and $C_{\mathrm{Sub}(B_1)-2N} = \{C_{2N\pi}, C_{6N\pi}, C_{10N\pi}\}$. The dependence of B_k on the corresponding C's can be determined from the above recursion relation.

In order to get the individual $C_{i\pi}$'s, $D_k^{(\tilde{n})}(\lambda_j)$ is required for three different λ_j's. Different choices of λ_j's have no effect on $C_{i\pi}$'s (we have confirmed this numerically). From the $D_k^{(\tilde{n})}(\lambda_j)$'s, the $C_{k\pi}$'s are extracted by solving the following equation, taking the block

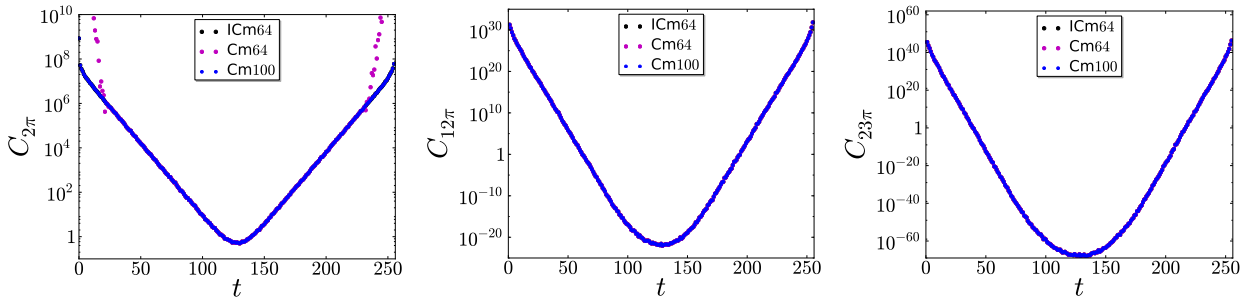

FIG. 1: $C_{2\pi}(t)$, $C_{12\pi}(t)$ and $C_{23\pi}(t)$ calculated from $N = 2$ sources by ICm with 64-decimal digital precision, denoted as ICm64, and Cm with 64(100)-decimal digital precision, denoted as Cm64(Cm100), on a single configuration are compared. Correlation functions from Cm100 agree with those from ICm64, however for the same precision, the ICm gives more accurate result than Cm. For $C_{2\pi}(t)$, Cm64 fails because of the numerical inaccuracy.

$[C_{4N\pi}, C_{8N\pi}, C_{12N\pi}]$ for example,

$$\begin{pmatrix} D_1^{(\tilde{n})}(\lambda_1) \\ D_1^{(\tilde{n})}(\lambda_2) \\ D_1^{(\tilde{n})}(\lambda_3) \end{pmatrix} = \begin{pmatrix} \lambda_1^{4N} & \lambda_1^{8N} & \lambda_1^{12N} \\ \lambda_2^{4N} & \lambda_2^{8N} & \lambda_2^{12N} \\ \lambda_3^{4N} & \lambda_3^{8N} & \lambda_3^{12N} \end{pmatrix} \cdot \begin{pmatrix} C_{4N\pi} \\ C_{8N\pi} \\ C_{12N\pi} \end{pmatrix}. \tag{13}$$

Inverting this matrix does not suffer from the numerical instabilities seen in the VMm, however as $12N$ becomes large, even computing the inverse of these 3×3 matrices requires high precision. Fig. 1 shows a comparison of the correlation functions computed from 2 sources by applying the Combination method and Improved Combination method to be discussed below. For the $N = 2$ Combination method, $C_{1\pi}(t)$, $C_{9\pi}(t)$ and $C_{17\pi}(t)$ are computed simultaneously by inverting a 3×3 matrix, similarly for ($C_{2\pi}(t)$, $C_{10\pi}$, $C_{18\pi}(t)$), and ($C_{3\pi}(t)$, $C_{11\pi}(t)$, $C_{19\pi}(t)$). Because of the large magnitude difference between $C_{1\pi}$ ($C_{2\pi}$, $C_{3\pi}$) and $C_{17\pi}$ ($C_{18\pi}$, $C_{19\pi}$), which becomes smaller for $C_{4\pi}$ ($C_{5\pi}$, $\cdots$) and $C_{20\pi}$ ($C_{21\pi}$, $\cdots$), at 64 digit precision, $C_{1\pi}(t)$, $C_{2\pi}(t)$ and $C_{3\pi}(t)$ show signs of numerical break down at earlier time slices, which goes away at higher precision (100 digit), indicating that even calculating the inverse of the 3×3 matrix needs high precision to get the correct results.

As constructed, this method is only applicable to a 2^n source problem. In order to solve problems having arbitrary number of sources, we extended this to an Improved Combination method in the next section.

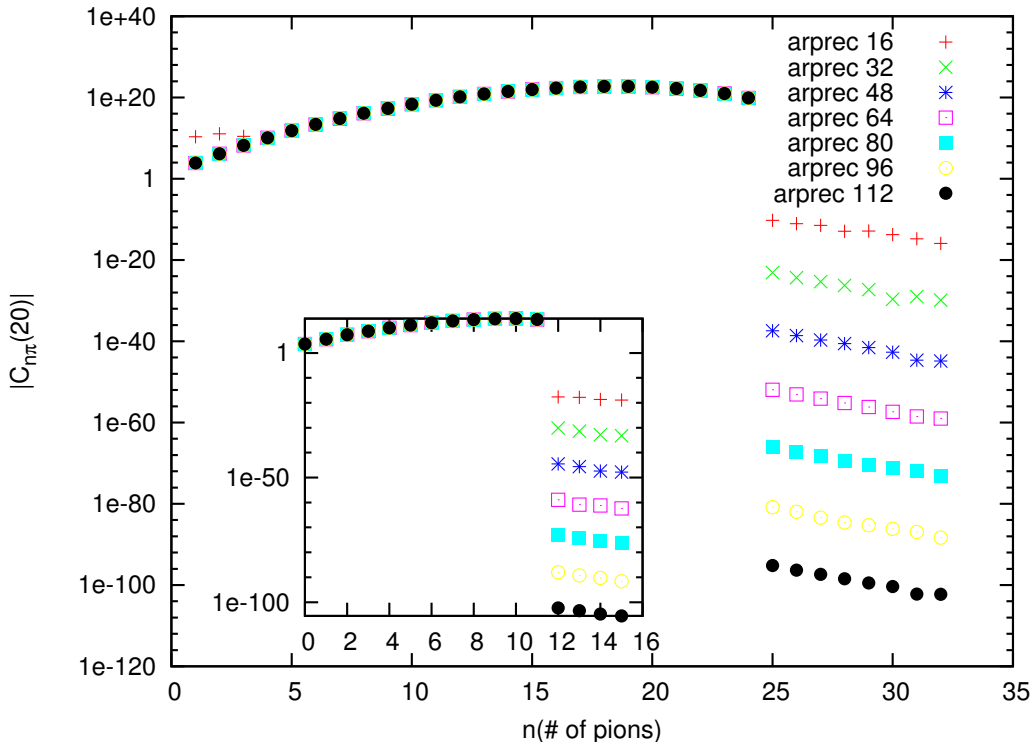

FIG. 2: Correlation functions on a single configuration at $t = 20$ from 2 sources computed with the Improved Combination method using the arprec library [19] at various precisions: 'arprec X' denotes that the calculation is done with X-decimal digit precision. The $C_{n\pi}(20)$ for $n = 1, 2, \ldots 24$ all agree for the different precision calculations just as they should, except for the calculation from 16-digit precision. However $C_{n\pi}(20)$ for $n = 25, 26, \ldots, 32$ are all machine zero at each precision. The disagreement of 16-digit precision indicates higher precision is needed. A similar comparison is shown for the single source correlation functions in the insert.

D. Improved Combination method (ICm)

As there are $12N$ terms in the expansion of $\det[1 + \lambda A]$, the Combination method does not allow us to determine functions depending on less than 3 $C_{k\pi}$'s. A similar problem appears in the application of the FFT. In order to use FFT, 2^n data points are required. If the number of points in a series is not equal to 2^n, points with value zero must be appended to the original series to produce a series of length 2^n. Similarly, we can append additional $C_{k\pi}$'s to the expansion of $\det[1 + \lambda A]$, as:

$$\det[1 + \lambda A] = 1 + \lambda C_{1\pi} + \lambda^2 C_{2\pi} + \ldots + \lambda^{12N} C_{12N\pi} + \lambda^{12N+1} C_{(12N+1)\pi} + \ldots + \lambda^{2^m} C_{2^m\pi}(14)$$

where $C_{p\pi} = 0$ for all $p > 12N$. The power m is chosen such that $2^{m-1} < 12N < 2^m$. With this new arrangement, exactly the same prescription discussed for the Combination Method can be applied, but in the last step the $D_k^{(\tilde{n})}(\lambda)$ individually depends only on a single correlation function.

A significant advantage of this method compared with the Cm is that no matrix inversion is required, so it is consequently less demanding in numerical precision, see Fig. 1, and in addition, problems with arbitrary numbers of sources can be solved with this method. Correlation functions appended to the series are solved for simultaneously with the other $C_{k\pi}$'s, providing a numerical check of the validity of this method. In Fig. 2, correlation functions calculated from 1-source and 2-sources on a single configuration are shown for different precision (we use the "arprec" library [19] to perform arbitrary precision calculations). As expected, all $C_{p\pi}$'s for $p > 12N$ are indeed numerically equivalent to zero, decreasing exponentially as the the numerical precision is increased. Since this method is more numerically stable than the Combination method, and can also solve problems of arbitrary number of sources, it is used in our further studies.

E. Generalization to 2 species from N sources

The methods discussed above can easily be generalized to two species by studying properties of the expansion of $\det[1 + \lambda_1 A + \lambda_2 B]$, where A and B are uncontracted correlation functions of two distinct species, for example π^+ and ρ^+. We can write

$$\det[1 + \lambda_1 A + \lambda_2 B] = 1 + \lambda_2^0 T_0 + \lambda_2^1 T_1 + \ldots + \lambda_2^k T_k + \ldots, \tag{15}$$

where

$$T_k(\lambda_1) = \lambda_1^0 C_{0A,kB} + \binom{k+1}{k} \lambda_1 C_{1A,kB} + \ldots + \binom{M}{k} \lambda_1^{M-k} C_{(M-k)A,kB}, \tag{16}$$

where $M = 12N$ is the dimension of the matrices A and B, and the correlation functions, $C_{mA,nB}$, are complicated combinations of correlation functions of a system having m-A's and n-B's distributed among different sources in all possible ways.

The $T_j(\lambda_1)$, for $j = 0, 1, \ldots, M$ for one λ_1 can be separated out by applying the methods discussed above with different choices of λ_2's, and then by applying the method again for different choices λ_1's for all $T_j(\lambda_1)$'s, the $C_{mA,nB}$'s can be separated out. This can be further generalized to correlators of arbitrary number of species as necessary.

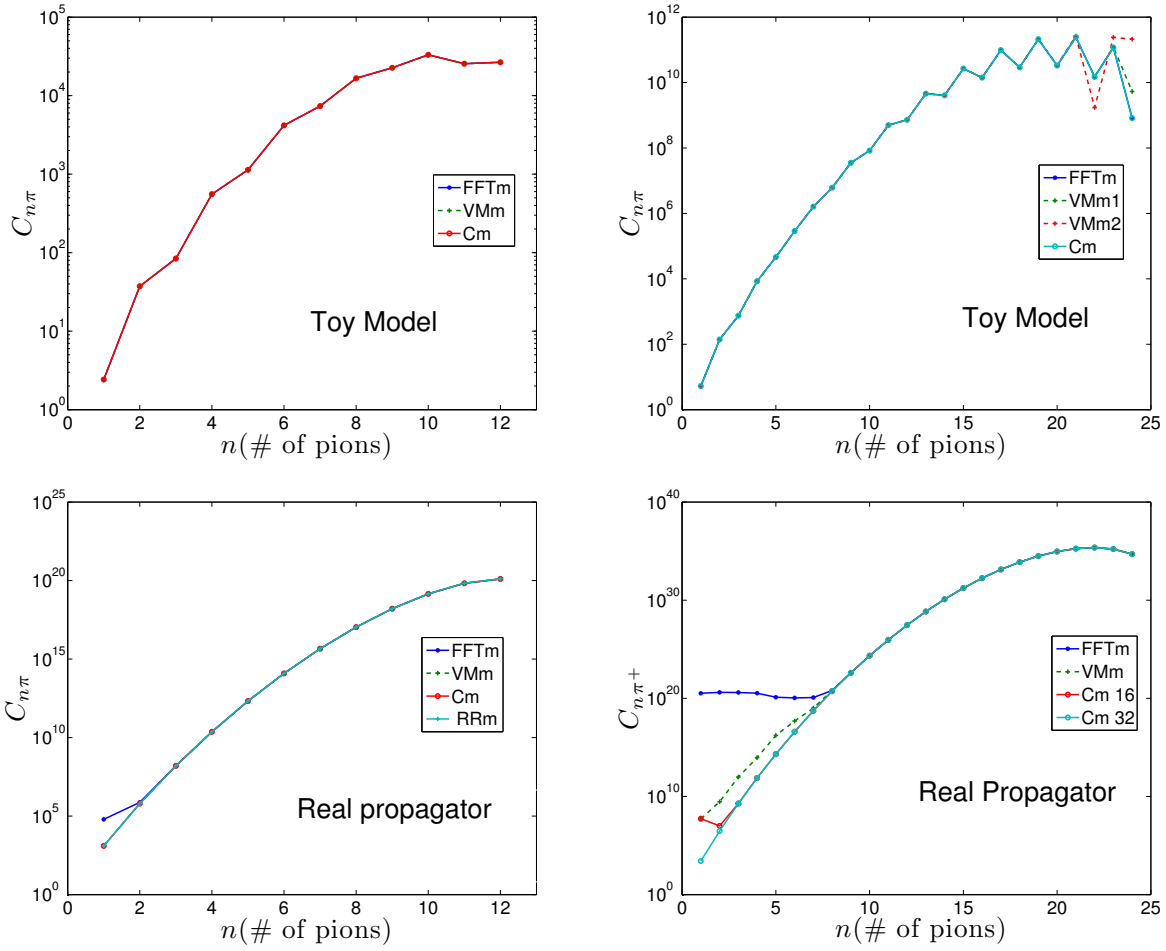

FIG. 3: The left panels compare 1-source calculations from the VMm, FFTm and Cm, and the right panels compare $C_{n\pi}$ calculated from 2 sources by the three methods. The real propagator is taken from one time slice, $t = 20$. The Recursion Relation method (RRm) [15] is also compared with other methods in the lower left plot as a check on the validity of the Cm. For the 2-source calculation in the toy model (top right) with VMm, two different sets of λ_ns have been used, denoted as VMm1 and VMm2. For VMm applied to the real propagator calculations, only one choice of λ's is shown. "Cm 16 (32)" denotes that calculation is done using Cm with 16(32) decimal digit precision.

F. Performance of different methods

In order to test the accuracy of different methods at a fixed precision, we compared correlation functions calculated from the VMm (implemented in MATLAB), the FFTm (implemented in MATLAB), and the Cm (implemented in C++ using the "arprec"

high precision library [19]). We first considered a toy model with matrix elements $A_{n,m} = \sin((m-1)(n-1)+2) + i\cos(2(n-1))$ for 1 and 2 sources in the top half of Fig. 3. For this test, the λ's used in the VMm and Cm are randomly chosen between -0.25 and 0.25, however $C_{n\pi}(t)$ should be independent of these choices. Results from VMm on 1-source agree with those from the FFTm and Cm for any set of λ. However for 2 sources, the FFTm and the Cm give the same results, but the VMm gives inconsistent results and changes with different choices of λ's, signaling a breakdown of the VMm and the requirement of higher precision. Similar tests have also been performed with the matrix elements $A_{n,m}$ extracted from real quark propagators and the results are shown in the lower half of Fig. 3. In this test, the Recursion Relation method (RRm) has also been used to compute the $C_{n\pi}$'s in order to validate the new methods. For the $N > 1$-source calculation no direct comparison with the RRm can be made, since the $C_{\overline{n}\pi}$ computed from the new methods are complicated combinations of all $C_{n_1,\ldots,n_N}$'s with $\sum_{i=1}^{N} n_i = \overline{n}$. We verified however that the energies extracted for these correlators with either method, RRm and Cm, are in agreement. In contrast to the toy model, for the real $A_{n,m}$, the VMm gives more accurate results than the FFTm. However both tests show that the Cm gives the most accurate results for a fixed precision. Tests with real propagators on 2-source shows a break down of Cm on $C_{1\pi}$ and $C_{2\pi}$, however this breakdown can easily be corrected by working at higher precision.

TABLE I: Scaling of different methods in terms of number of multiplications for an N source calculation.

	scaling
RRm	$12^4 N^4 \exp(2.8(N-1))$
VMm	$(12N+2)(12N)^3$
Cm	$3 \cdot 2^{\log 2(4N)}(12N)^3$
ICm	$2^{\mathrm{floor}(\log_2(12N))+2}(12N)^3$

The main purpose of constructing these new methods is to expedite the contractions required in computing correlation functions for systems comprised large number of mesons. The numerical scaling of the Recursion Relation method, Vandermonde Matrix method, Combination method and Improved Combination method (the FFT method costs the same amount of time as the ICm if f_0, τ and T are chosen appropriately) are com-

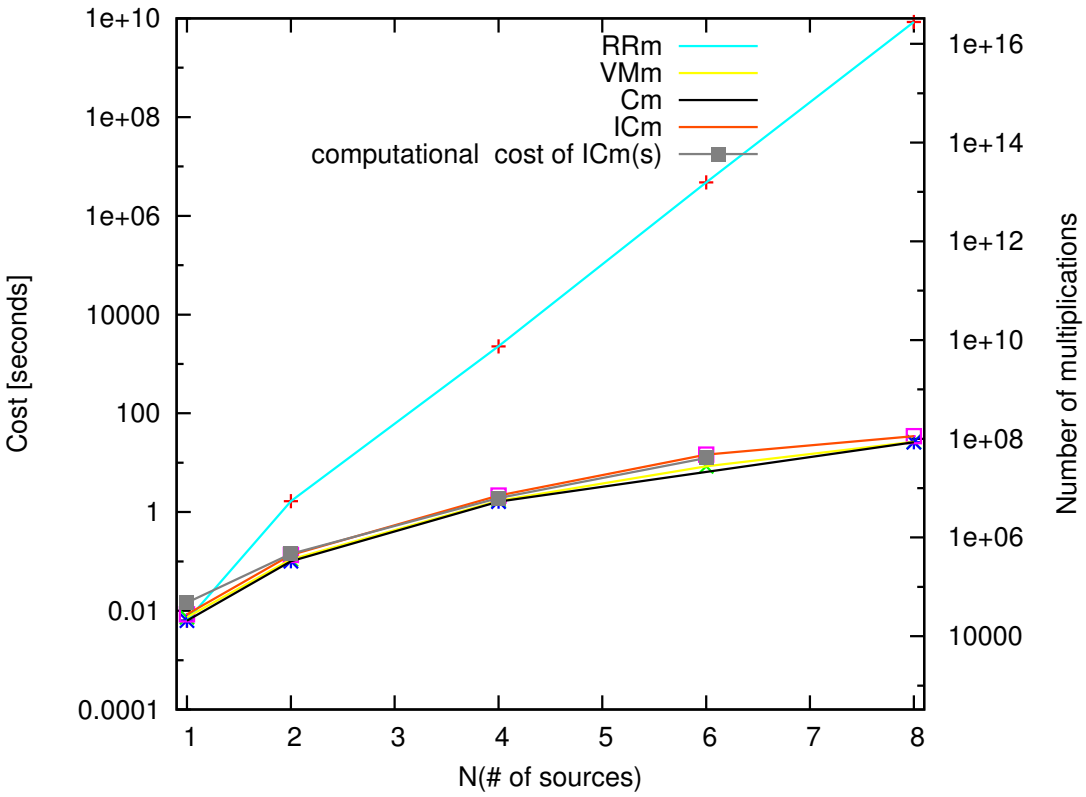

FIG. 4: Comparison of the number of multiplications required for each method (RH axis), and the corresponding computation time of $C_{n\pi}(t)$ for $n = 1, 2, \ldots 12N$ on a single time slice, corresponding to one application of the specified contraction method in seconds using a single 2.4 GHz Xeon core (LH axis). The computational cost of the ICm is taken from the actual running time, and it is used to normalize the time scale so that the projected running time of other methods can be read out from the LH axis.

pared in Table I. For each method, we determine how many multiplications are required. From Ref. [15], the computational cost of the recursion relation method is proportional to $12^4 N^4 \exp(2.8(N-1))$, where N is the number of sources. The VMm requires a calculation of $12N$ determinants, one inversion of $12N \times 12N$ matrix and the multiplication of a $12N \times 12N$ matrix and $12N \times 1$ vector. The dominant contribution to the computational cost of the other two methods comes from calculating a large number of determinants. For the Improved Combination method, a step-n calculation requires the computation of 2^n determinants, while the Combination method requires $3 \cdot 2^n$ for a step-n calculation. To solve an N-source problem, the Combination method requires $\log 2(4N)$ steps for $N = 2^m$, where

m is an integer, and the Improved Combination method requires floor($\log_2(12N)$) + 2 steps. Taking account of all the determinant calculations that are needed, and the computational cost of each determinant ($\sim (12N)^3$ using LU decomposition), the numerical cost of each method is tabulated in Table. I, and compared in Fig. 4. Although the recursion relation method significantly reduces the cost of contractions over the original $(12N!)^2$ scaling, the computational cost of the recursion relation method is much larger than other methods, all of which scale similarly. Using the ICm, we now turn to our numerical investigations of systems of large number of mesons.

III. LATTICE DETAILS

The calculations in this paper are performed on ensembles of anisotropic gauge field configurations with clover-improved fermions [21] that have been generated by the Hadron Spectrum Collaboration and the Nuclear Physics with Lattice QCD collaboration. The gauge action is a tree-level tadpole-improved Symanzik-improved action, and the fermion action [22, 23] is a $n_f = 2 + 1$ anisotropic clover action [24] with two levels of stout smearing [25] with weight $\rho = 0.14$ only in spatial directions (see [17] for more details). In order to preserve the ultra-locality of the action in the temporal direction, no smearing is performed in that direction. Furthermore, the tree-level tadpole-improved Symanzik gauge action without a 1×2 rectangle in the time direction is used.

Four ensembles of gauge fields are used in this paper with volumes $L^3 \times T$ of $16^3 \times 128$, $20^3 \times 128$, $24^3 \times 128$ and $20^3 \times 256$, and with a renormalized anisotropy $\xi = a_s/a_t = 3.5$, where a_s (a_t) is the spatial (temporal) lattice spacing. The lattice spacing is the same for each ensemble and is $a_s = 0.1227 \pm 0.0008$ fm [17], which gives spatial extents $L \sim 2.0, 2.5, 3.0$ fm for $L = 16, 20, 24$ respectively. The same input light quark mass $a_t m_l = -0.0840$ and input strange quark mass $a_t m_s = -0.0743$ are used in generating each ensemble, giving a pion mass of $m_\pi \sim 390$ MeV and a kaon mass of $m_K \sim 540$ MeV. The quantities $m_\pi L$ and $m_\pi T$, which determine the impact of the finite volume and temporal extent, are $m_\pi L \sim 3.86, 4.82, 5.79$ for $L = 16, 20, 24$ lattices and $m_\pi T \sim 8.82, 17.64$ for $T = 128, 256$, respectively. Details of the four ensembles are summarized in Table II.

In our work, a momentum space representation of the contractions is used and Coulomb gauge fixed propagators in time-momentum space, which we refer to as "colorwave propa-

TABLE II: Details of the four gauge ensembles with the same lattice space $a = 0.1227 \pm 0.0008$ fm used in this paper. $N_{\rm cfg}$ denotes the number of configurations used in the current calculation. In the last two columns, $N_{\rm src}$ is the number of source times used on each configuration and $N_{\rm mom}$ is the number of momentum sources used for each source time.

	$L^3 \times T$ (a^{-1})	L (fm)	$m_\pi L$	$m_\pi T$	$N_{\rm cfg}$	$N_{\rm src}$	$N_{\rm mom}$
B1	$16^3 \times 128$	2.0	3.9	8.8	180	8	33
B2	$20^3 \times 128$	2.5	4.8	8.8	51	8	19
B3	$24^3 \times 128$	3.0	5.8	8.8	98	8	19
B4	$20^3 \times 256$	2.5	4.8	17.6	147	16	7

gators", $S_{u/d}(\mathbf{p}, \tau; \mathbf{p'}, 0)$, are calculated on each configuration[2]. The colorwave propagator is defined as

$$S_{u/d}(\mathbf{p}, t; \mathbf{p'}, 0) = \sum_{\mathbf{y}} e^{-i\mathbf{px}} S_{u/d}(\mathbf{x}, t; \mathbf{p'}, 0), \tag{17}$$

where

$$S_{u/d}(\mathbf{x}, t; \mathbf{p'}, 0) = \sum_{\mathbf{y}} e^{i\mathbf{p'y}} S_{u/d}(\mathbf{x}, t; \mathbf{y}, 0),$$

is a solution of the Dirac equation:

$$\sum_{\mathbf{x},t} D(\mathbf{y}, \tilde{t}; \mathbf{x}, t) S_{u/d}(\mathbf{x}, t; \mathbf{p'}, 0) = e^{i\mathbf{p'y}} \delta_{\tilde{t},0}.$$

The colorwave propagator, $S_{u/d}(\mathbf{p}, \tau; \mathbf{p'}, 0)$ describes a quark propagating from the source $(\mathbf{p'}, 0)$ to the sink $(\mathbf{p}, \tau)$ in time-momentum space. The colorwave propagator and the position space propagator are related by a 3 dimensional Fourier transformation as follows:

$$S_{u/d}(\mathbf{p}, t; \mathbf{p'}, 0) \; = \; \sum_{\mathbf{xy}} \quad e^{-i\mathbf{px}} \quad e^{i\mathbf{p'y}} \quad S_{u/d}(\mathbf{x}, t; \mathbf{y}, 0), \tag{18}$$

and the conjugate of a propagator is $S^\dagger(-\mathbf{p}, t; -\mathbf{p'}, 0) = \gamma_5 S(\mathbf{p'}, 0; \mathbf{p}, t) \gamma_5$. The γ_5 hermiticity of the colorwave propagator follows from the γ_5 hermiticity of its counterpart in position space.

[2] As we compute gauge invariant quantities, our results are independent of the gauge fixing procedure.

A correlation function of one pion with momentum $\mathbf{p}_f$ can be constructed by projecting both sink and source to the same momentum $\mathbf{p}_f$ as:

$$\begin{aligned} C_{1\pi}(\mathbf{p}_f,t) &= \left\langle \sum_{\mathbf{x},\mathbf{x}'} e^{-i(\mathbf{p}_1\mathbf{x}-\mathbf{p_2}\mathbf{x}')}\overline{d}(\mathbf{x}',t)\gamma_5\ u(\mathbf{x},t)\ \sum_{\mathbf{y}\mathbf{y}'}\ e^{i\mathbf{p}\mathbf{y}}e^{-i(\mathbf{p}-\mathbf{p}_f)\mathbf{y}'}\ \overline{u}(\mathbf{y},0)\gamma_5 d(\mathbf{y}',0)\right\rangle \\ &= \sum_{\mathbf{x},\mathbf{x}',\mathbf{y},\mathbf{y}'} \left\langle e^{-i\mathbf{p}_1\mathbf{x}}e^{i\mathbf{p}\mathbf{y}}\ \gamma_5 S_u(\mathbf{x},t;\mathbf{y},0)\ \gamma_5 e^{i\mathbf{p}_2\mathbf{x}'}\ \ e^{-i(\mathbf{p}-\mathbf{p}_f)\mathbf{y}'}\ (\gamma_5 S_d^\dagger(\mathbf{x}',t;\mathbf{y}',0)\gamma_5)\right\rangle \\ &= \left\langle \sum_{\mathbf{x},\mathbf{y}}\ \gamma_5(e^{-i\mathbf{p}_1\mathbf{x}}e^{i\mathbf{p}\mathbf{y}}S_u(\mathbf{x},t;\mathbf{y},0))\sum_{\mathbf{x}',\mathbf{y}'} e^{-i(\mathbf{p}-\mathbf{p}_f)\mathbf{y}'}e^{i\mathbf{p}_2\mathbf{x}'}\gamma_5(\gamma_5 S_d^\dagger(\mathbf{x}',t;\mathbf{y}',0)\gamma_5)\right\rangle \\ &= \left\langle \gamma_5 S_u(\mathbf{p}_1,t;\mathbf{p},0)\cdot\gamma_5(\gamma_5 S_d^\dagger(-\mathbf{p}_2,t;\mathbf{p}_f-\mathbf{p},0)\gamma_5)\right\rangle, \end{aligned} \tag{19}$$

where $\mathbf{p}_1-\mathbf{p}_2=\mathbf{p}_f$. Each choice of $\{\mathbf{p}_1,\mathbf{p}_2\}$ and $\mathbf{p}$ satisfying momentum conservation is a separate correlation function with distinct creation and annihilation interpolating fields, and we have suppressed the dependence of $C_{1\pi}$ on $\mathbf{p}_1$, $\mathbf{p}_2$ and $\mathbf{p}$. During the calculation, we held $\mathbf{p}_1$, $\mathbf{p}_2$ and $\mathbf{p}_f$ fixed and summed over all $\mathbf{p}$'s for which we have computed colorwave propagators (see Table. II) in order to get more statistics. In the second step, the definition of propagator $S_{u/d}(\mathbf{x}',t;\mathbf{y},0)$ and the γ_5 hermiticity of the propagator is used. The definition of the colorwave propagator, Eq. (18), is applied in the last step.

The correlation functions of a system having n π^+'s in a single source, with total momentum $\mathbf{P}_f=n\ \mathbf{p}_f$ can be constructed similarly:

$$\begin{aligned} C_{n\pi}(t,\mathbf{P}_f) &= \left\langle \left(\sum_{\mathbf{x},\mathbf{x}'} e^{-i(\mathbf{p}_1\mathbf{x}-\mathbf{p_2}\mathbf{x}')}\overline{d}(\mathbf{x}',t)\gamma_5 u(\mathbf{x},t)\right)^n \right. \\ &\quad \left. \cdot\left(\sum_{\mathbf{y},\mathbf{y}'} e^{i\mathbf{p}\mathbf{y}}e^{-i(\mathbf{p}-\mathbf{p}_f)\mathbf{y}'}\overline{u}(\mathbf{y},0)\gamma_5 d(\mathbf{y}',0)\right)^n\right\rangle, \end{aligned} \tag{20}$$

where the dependence of $C_{n\pi}$ on $\mathbf{p}_1$, $\mathbf{p}_2$ and $\mathbf{p}$ has also been suppressed in Eq. (20).

Because of the Pauli exclusion principle, systems constructed from a single source in momentum space can only reach a maximum of 12 π^+'s. In order to put more pions into a system, additional sources are required. Correlation functions of a N-source system having $\overline{n}=\sum_{i=1}^N n_i\pi^+$'s with total momentum $\mathbf{P}_f=\sum_{i=1}^{\overline{n}}\mathbf{p}_{f_i}$ are given by

$$\begin{aligned} C_{n_1\pi,\ldots,n_N\pi}(t,\mathbf{P}_f) &= \left\langle \prod_{i=1}^N\left(\sum_{\mathbf{x}_i,\mathbf{x'}_i} e^{-i(\mathbf{p}_1^i\mathbf{x}_i-\mathbf{p}_2^i\mathbf{x'}^i)}\overline{d}(\mathbf{x'}_i,t)\gamma_5 u(\mathbf{x}_i,t)\right)^{n_i}\right. \\ &\quad \left.\times\ \prod_{j=1}^{\overline{n}}\left(\sum_{\mathbf{y}_j,\mathbf{y}'_j} e^{i\mathbf{p}_j\mathbf{y}_j}e^{-i(\mathbf{p}_j-\mathbf{p}_{f_j})\mathbf{y}'_j}\overline{u}(\mathbf{y}_j,0)\gamma_5 d(\mathbf{y}'_j,0)\right)\right\rangle, \end{aligned} \tag{21}$$

where n_i is the number of pions in the i^{th} source, and momentum conservation $\sum_{i=1}^{N} n_i(\mathbf{p}_1^i - \mathbf{p}_2^i) = \sum_{j=1}^{\overline{n}} \mathbf{p}_{f_j}$, must be satisfied in order for the correlation functions to be non-vanishing. In the current work, only systems with total zero momentum, $\mathbf{P}_f = (0,0,0)$, are investigated, and $\mathbf{p}_{f_j}$'s for each source are also fixed to $\mathbf{p}_{f_j} = (0,0,0)$[3]. The contraction methods discussed in the last section apply equally well in momentum space and are used in our work. The elements of the counterpart of uncontracted correlation functions defined in Eq. (2) are:

$$\tilde{A}_{k,i}(t) = \sum_{\mathbf{p}} S\left(\mathbf{p}_1^k, \mathbf{p}\right) S^{\dagger}\left(-\mathbf{p}_2^i, \mathbf{p}_{f_i} - \mathbf{p}\right), \tag{22}$$

where k, i label the source and sink, and the dependence on $\mathbf{p}_1^k$, $\mathbf{p}_2^i$, $\mathbf{p}$ and $\mathbf{p}_{f_i}$ is suppressed.

For the $T = 128$ (256) ensembles, 8 (16) colorwave propagators are generated on each configuration located 16 time slices apart to minimize correlations between propagators. For ensembles $\{B1, B2, B3, B4\}$, $\{180, 51, 147, 98\}$ configurations and $\{33, 19, 19, 7\}$ momenta are used respectively. In order to reduce contamination from thermal states, a temporal extent of $T = 256$ is desirable for systems of large numbers of pions. On the B1 and B3 ensembles, the $A \pm P$ (antiperiodic $\pm$ periodic propagator) method [26–28] is applied to effectively double the temporal extent. The validity of this method is investigated by comparing results from ensemble B4 ($20^3 \times 256$) and with those from ensemble B2 ($20^3 \times 128$) with the $A \pm P$ method and it is found to be sound at the precision we achieve for the systems under consideration as discussed below.

IV. GROUND STATE ENERGIES

Previous studies of the energies and isospin chemical potentials [6, 16] on ensemble B2 showed that thermal states contribute significantly to correlation functions and, even for $C_{12\pi}(t)$, the ground state does not dominate in any region of Euclidean time. The expected

[3] Using non-zero momentum sources, for example $\mathbf{p}_{f_1} = (0,0,-1)$ and $\mathbf{p}_{f_2} = (0,0,1)$, to construct a zero momentum system has also been investigated, and we find that higher momenta sources have smaller contribution to the correlation function of a system at rest than zero momentum sources. Technically, different weights can be chosen in Eq. (21) for each combination of $\mathbf{p}_{f_i}$ to get better overlap to the ground state.

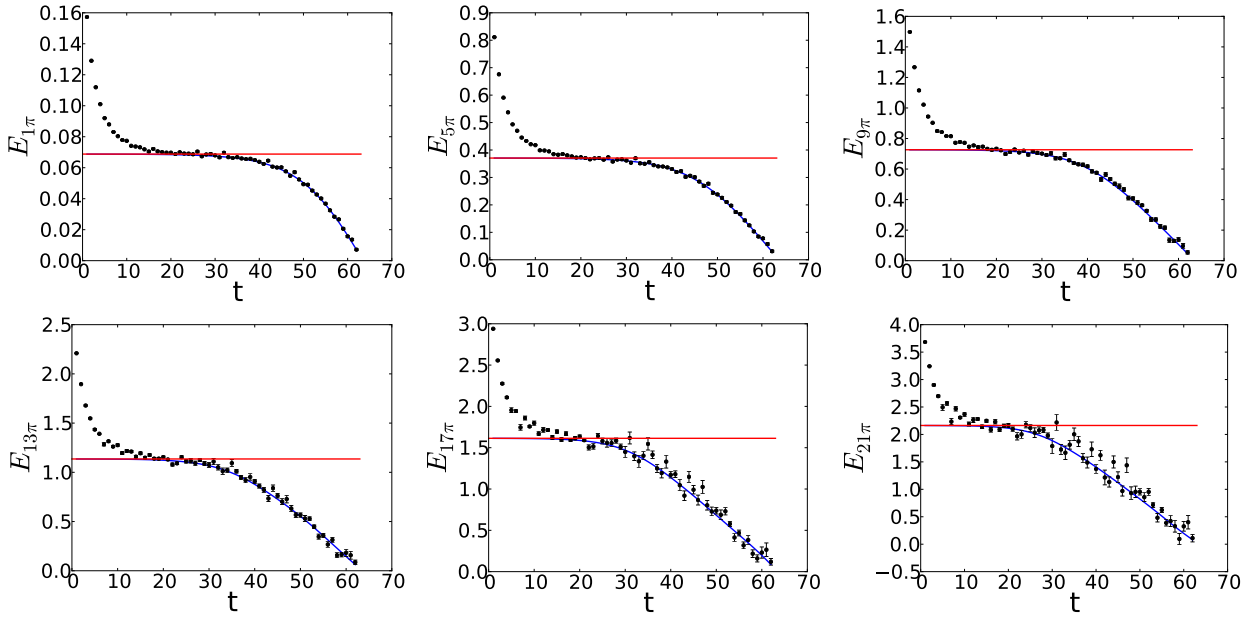

FIG. 5: The black data is the effective mass calculated from the original data from ensemble B2, and blue line is reconstructed from the ground state energies extracted from the ensemble B4 as discussed in the main text. The red line is the fitted value of $E_{n\pi}$ extracted from the correlators of ensemble B4.

form of correlation functions of an n-π^+ system with temporal extent T is [6]

$$C_{n\pi}(t) \;=\; \sum_{m=0}^{\lfloor \frac{n}{2} \rfloor} \binom{n}{m} A_m^n Z_m^n e^{-(E_{n-m}+E_m)T/2} \cosh((E_{n-m}-E_m)(t-T/2)) + \ldots, \qquad (23)$$

where $A_m^n = 1$ when $m = n/2$, otherwise $A_m^n = 2$. E_m is the ground state energy of a m-π^+ system, the Z_m^n are the overlap factors for contribution with m π's propagating backward around the temporal boundary, and the ellipsis denotes contributions from excited states. The ground state contribution comes from the $m = 0$ term, and thermal states are from the $m \neq 0$ terms in the sum, corresponding to contributions where m π^+'s propagate backwards from the source to the sink around the temporal boundary. For the $T = 128$ B2 ensemble, effective mass plots are shown in Fig. 5 for various n, and it is clear that correlation functions receive significant contributions from thermal states. Their analysis requires a fit including all thermal states, Eq. (23), in order to extract the ground state energy. Since the number of free parameters in the fit grows with n, the systematic uncertainty of $E_{n\pi}$ becomes large and we are unable to extract any accurate information at large n. In order to minimize contributions from thermal states, a longer temporal extent is required.

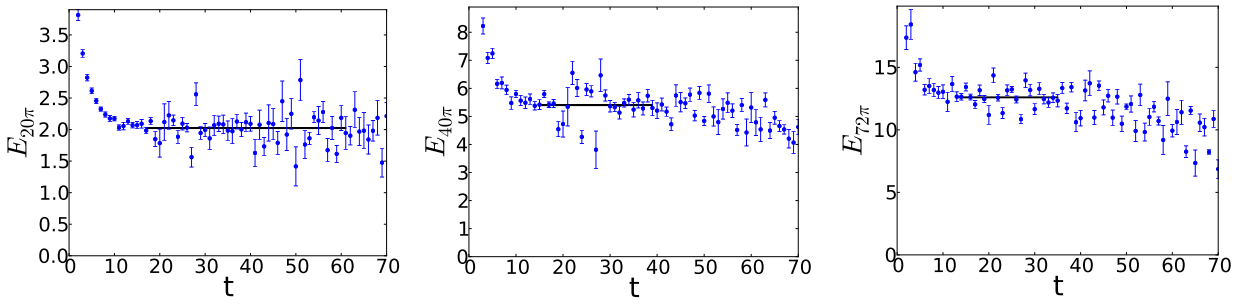

FIG. 6: The effective mass of $C_{20\pi}(t)$ from the 2-source calculation on the ensemble B4 is shown on the left along with the extracted ground state energy represented as a black band. Similarly, the effective mass of $C_{40\pi}(t)$ ($C_{72\pi}(t)$) from the 4 (6) source calculation on the same ensemble and the corresponding extracted ground state energy is shown in the middle (on the right).

Thermal effects are exponentially suppressed by the larger temporal extent and the ensemble with $T = 256$ has greatly reduced contamination, and a simple single exponential fit at intermediate times is sufficient to extract ground state energies, even for $E_{72\pi}$, as shown in Fig. 6. Effective mass plots of $C_{20\pi}$, $C_{40\pi}$ and $C_{72\pi}$ for this ensemble all show a plateau region, and a single exponential fit, only including the term in Eq. (23) with $m = 0$, is enough to extract the ground state energy $E_{n\pi}$. However, for significantly larger numbers of pions, a still larger temporal extents would again be necessary.

A. Energies from $20^3 \times 256$ ensemble

Correlation functions, defined in Eq. (21), for systems with the quantum numbers of up to 72 π^+'s have been computed on the B4 ensemble. In this paper, only systems having zero center of mass momentum are investigated. For a discussion of results for different total momenta, see Ref [16]. Because of precision issues, we have computed correlation functions from 2, 4, and 6 sources, from which $E_{1\pi\to 24\pi}$, $E_{25\pi\to 48\pi}$ and $E_{49\pi\to 72\pi}$ have been extracted respectively, where $E_{n\pi}$ is the ground state energy of a n-π^+ system at rest. Fig. 7 shows $C_{20\pi}(t)$, $C_{40\pi}(t)$ and $C_{70\pi}(t)$ from 6-source contractions. The breakdown at earlier time slices of $C_{20\pi}(t)$ indicates that computations with higher precision are required. Computations with arbitrary precisions are accessible with the "arprec" library [19], however at the same precision, they are ~ 5 times more expensive than with the fixed quad-double precision (implemented using the "qd" library [20]). In our main studies, we perform all contractions

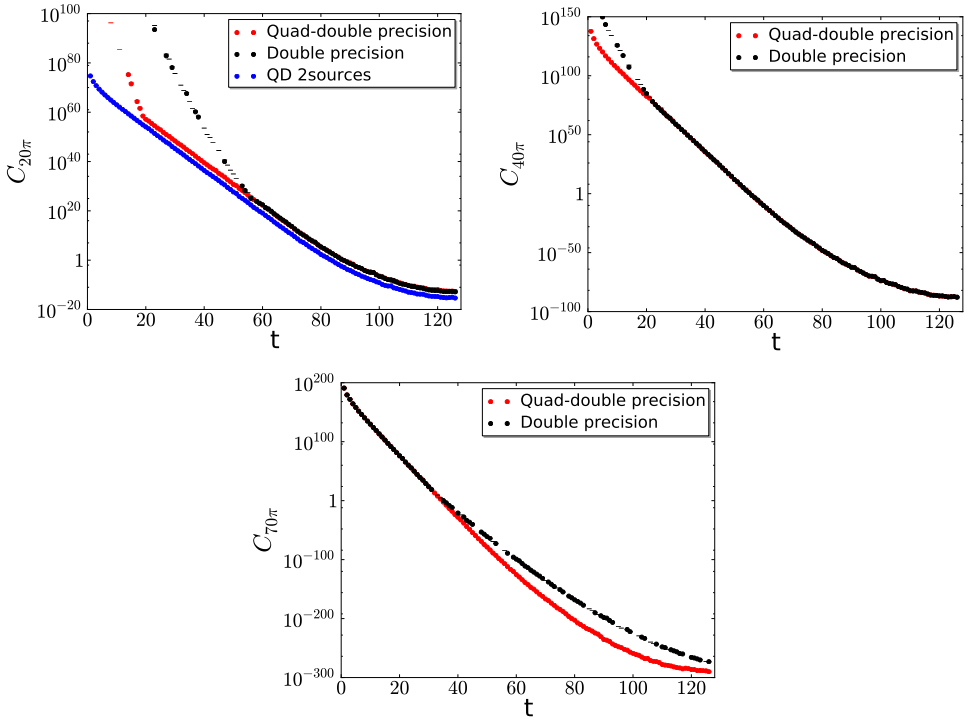

FIG. 7: The correlation functions, $C_{20\pi}(t)$, $C_{40\pi}(t)$ and $C_{70\pi}(t)$, calculated from 6-sources with quad-double precision and double precision are compared in the left, center, and right plots respectively. The same calculations done with double precision shows even more severely breakdown, indicating that high precision is needed in order to study many pion systems. Although $C_{20\pi}$ from 6-sources with quad-double precision breaks down at earlier time slices, the rescaled $C_{20\pi}$ from 2-source computations, which is shown also in the left plot, is free from precision issues and is used in extracting the $E_{20\pi}$.

in quad-double precision, and multiply the uncontracted propagators by a prefactor before performing the contractions such that the particular $C_{n\pi}(t)$'s that we focus on do not suffer from the limit of the floating point dynamical range of Quad-double precision (this prefactor is removed at the end of the calculation).

As the correlation functions of systems containing many pions span a large numerical range, $10^{250} \sim 10^{-250}$ for $C_{70\pi}(t)$ for example, inverting the correlation matrix during a correlated fit brings in significant instabilities, thus $E_{n\pi}$ for $n = 1, 2, \ldots 72$ are extracted from uncorrelated fits in this study. The fitting window is chosen between time slices where a clear plateau region of the effective mass plot can be seen. Statistical uncertainties are constructed from fits to multiple bootstrap resamplings of the ensemble (we use $N_s = 88$

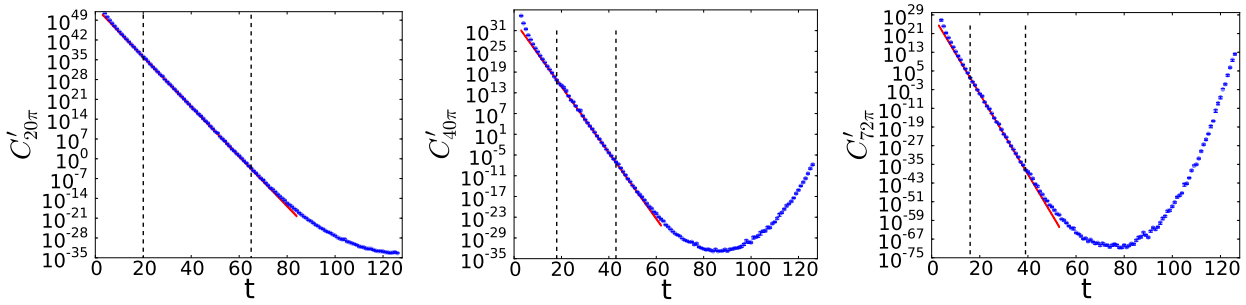

FIG. 8: $C'_{20\pi}(t)$ is shown on the left, where the blue points are data, the red line is constructed from the fit, and two vertical dashed lines indicate the fitting window. Similar plots of preconditioned $C'_{40\pi}(t)$ and $C'_{72\pi}(t)$ are also shown.

samples), and systematic uncertainties are estimated by shifting the fitting window forward and backward two time slices.

Since the ground state energy of a system containing many pions becomes large, even fitting correlation functions with only one exponential becomes problematic because of precision. Taking the 25-π^+ system for example, the ground state energy of this system is $E_{25\pi} = 2.76$ in temporal lattice units, and the fit is performed between $t/a_t = [15, 58] \pm 2$. The correlation function varies over 140 orders of magnitude from $t = 15$ to $t = 58$. Such a large change in magnitude requires care with precision and in order to ameliorate this problem, instead of fitting correlation functions directly, we fit the following preconditioned correlation functions:

$$C'_{n\pi}(t) = Z'_n \exp(\delta E_n t) C_{n\pi}(t), \tag{24}$$

where $C_{n\pi}(t)$ is the original correlation function, and Z'_n, and δE_n are fixed numbers, chosen so that $C'_{n\pi}(t)$ changes less dramatically inside the fitting window. Since the original correlation function behaves like a single exponential inside the plateau region where the ground state dominates, multiplying another exponential will not change this feature. Furthermore, the extracted ground state energy should have no dependence on Z'_n and δE_n, which is numerically confirmed. The preconditioned correlation functions and the corresponding single exponential fits for $n = 20, 40$ and 72 are shown in Fig. 8.

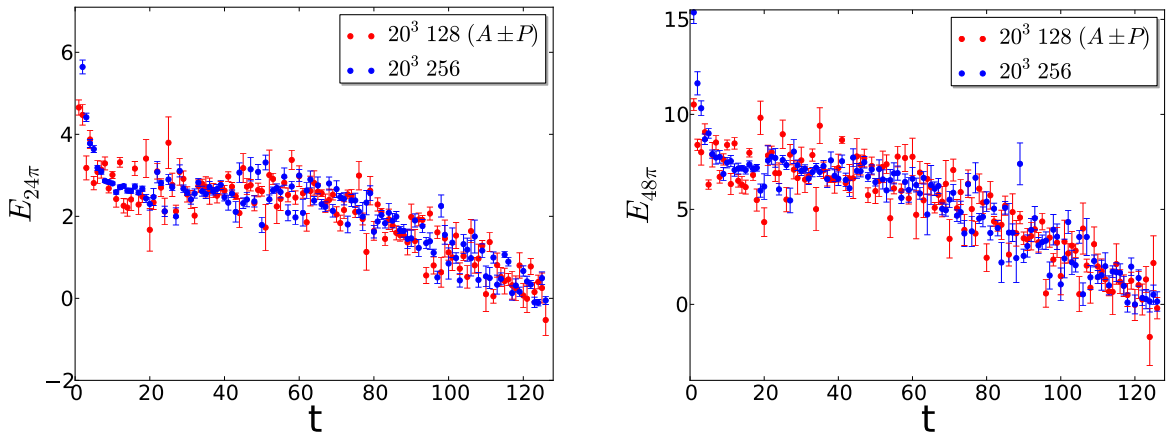

FIG. 9: Effective mass plots for $24\pi^+$ and $48\pi^+$ correlators. The blue data are from ensemble B4 and the red data are from the $A \pm P$ method on ensemble B2. Effective mass plots are consistent between these two calculations for all n π^+ systems.

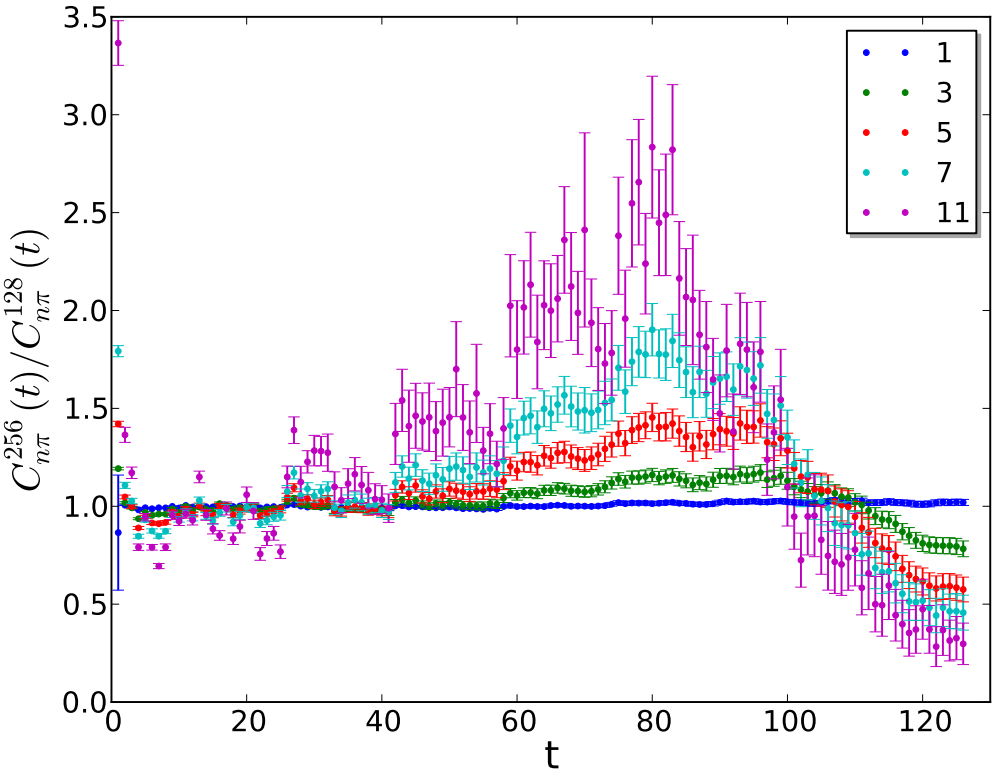

FIG. 10: The ratio of the correlation function of n π^+'s calculated by using the $A \pm P$ method on B2 ensemble, $C^{128}_{n\pi}(t)$, compared with that from B4 ensemble, $C^{256}_{n\pi}(t)$, for $n = 1, 3, 5, 7, 11$, is shown.

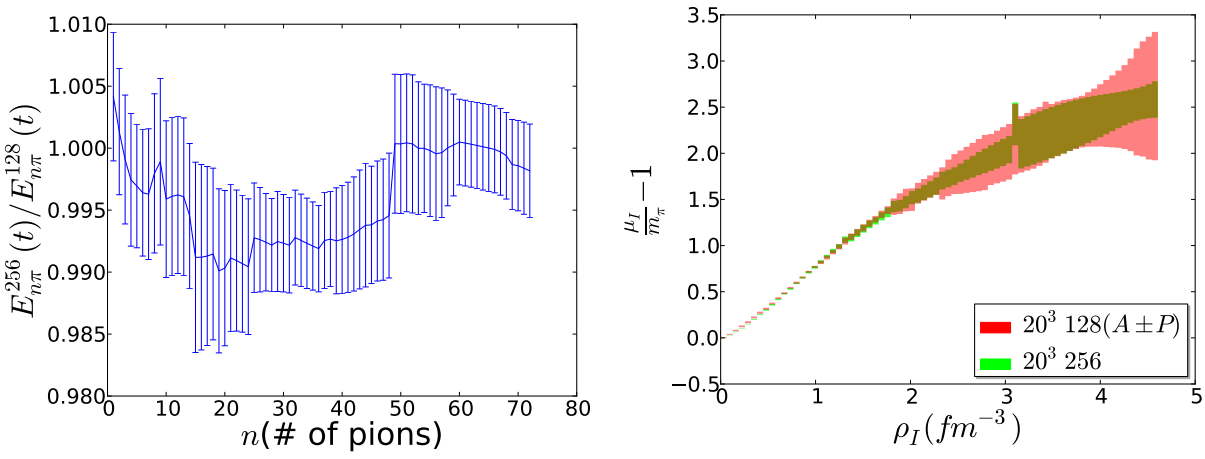

FIG. 11: The ground state energies, $E_{n\pi}$, extracted from ensemble B2 ($E_{n\pi}^{128}$) with $A \pm P$ method are compared with those from ensemble B4 ($E_{n\pi}^{256}$) in the left plot, where the ratio of $E_{n\pi}^{256}/E_{n\pi}^{128}$ is plotted. The isospin chemical potentials, μ_I, at different densities for the two ensembles are compared in the right plot.

B. Antiperiodic ± Periodic propagator method ($A \pm P$ method)

By keeping all Z_m^n factors the same as the ground state Z_0^n extracted from the B4 ensemble, we have reconstructed the correlators corresponding to the B2 ensemble by utilizing the ground state energies extracted from the B4 ensemble[4]. In Fig. 5, the reconstructed effective masses are compared with those from the correlation functions computed from the B2 ensemble, showing agreement within uncertainties. The contamination from the thermal states on the $T = 128$ (B2) ensemble can clearly be seen in the rate at which the plateau region (where the ground state energy dominates) shrinks as n increases. For systems with a large number of pions, excited states have not died out before thermal states become important.

Since a temporal extent $T \geq 128$ is required to get a clean signal for many-pion ground state energies, we have investigated the use of the $A \pm P$ method (combining propagators that satisfy anti-periodic and periodic boundary conditions in the temporal direction to cancel certain modes [26–28]). On the $T = 128$ B2 ensemble, we check the validity of this method in comparison to the B4 ($T = 256$) ensemble. In order to see the deviation

[4] While we do not expect $Z_m^n = Z_0^n$ for all m because of the effects of pion interactions, deviations are expected to be small (This is also supported by thermal fits using Eq. (23) for small n.).

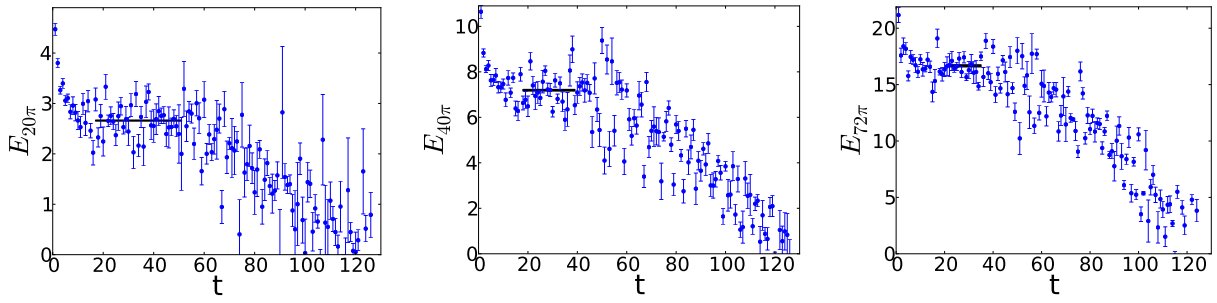

FIG. 12: Effective mass plots with $A \pm P$ method on ensemble B1 are shown here. The effective mass of $C_{20\pi}(t)$ from the 2-source calculation is shown on the left along with the ground state energy represented as a black band. Similarly effective mass plots of $C_{40\pi}$ from 4-sources and $C_{72\pi}(t)$ from 6-sources calculations and the extracted ground state energies are shown in the middle and right respectively.

of this method compared with those calculated directly from the $T = 256$ ensemble with anti-periodic boundary conditions in the temporal direction, effective mass plots from the two ensembles are compared in Fig. 9, and the ratio of correlation functions from these two methods are shown in Fig. 10. The $A \pm P$ method relays on the exact cancellation of thermal contributions, and is seen to work very well 1 π^+ system, see Fig. 10. For systems with more than 1 π^+, the $A \pm P$ method starts fail at later time slices, however it still gives consistent results at earlier time slices, where ground state energies can be extracted. Energies and isospin chemical potentials extracted from the $A \pm P$ method are compared with those from ensemble B4 in Fig. 11, which shows that the disagreement of extracted ground energies below 1%, and at our current precision, the $A \pm P$ method provides reliable results for the correlators we study. This gives us confidence to use the $A \pm P$ method for ensembles B1 and B3, where we could otherwise not extract ground state energies for large number of pions.

C. Energies from $16^3 \times 128$ and $24^3 \times 128$ ensembles

As the $A \pm P$ method has been validated on the B2 ensemble, systems having up to 72 π^+'s has also been studied on ensembles B1 and B3 using this method. Effective mass plots with extracted ground state energies from ensemble B1 are shown in Fig. 12 and those from ensemble B3 are shown in Fig. 13. All calculations are done with the ICm, and ground

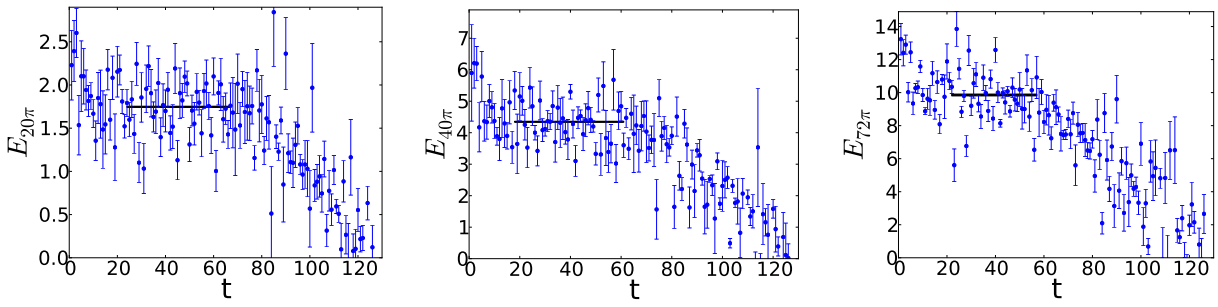

FIG. 13: Effective mass plots with $A \pm P$ method on ensemble B3 are shown.

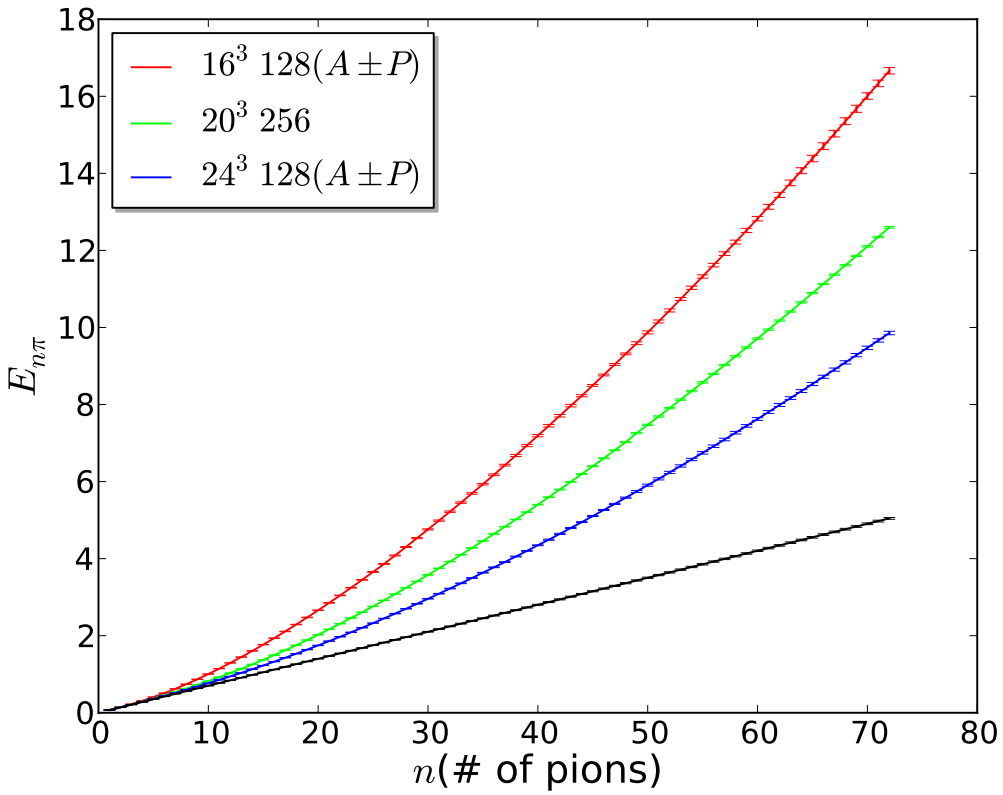

FIG. 14: The ground state energies of a system of n-π^+($E_{n\pi}$) extracted from ensembles B1 (red), B3 (blue) and B4 (green) are shown. The black line represents the total energy of n non-interacting pions.

state energies are extracted with the same statistical method as those in the Section IV A. The extracted ground state energies from all three volumes are shown in Fig. 14.

V. INTERACTION PARAMETERS

By considering the energy shifts of two particle states in a finite volume, $\Delta E \equiv E_2 - 2E_1 = 2\sqrt{\mathbf{p}^2 + m_\pi^2} - 2E_1$, Lüscher derived a relationship between the phase shift, $\delta(p)$, and the interacting momentum, $p = |\mathbf{p}|$, given by [29, 30] (see also [31]),

$$p \cot \delta(p) \;=\; \frac{1}{\pi L}\, \mathbf{S}\left(\left(\frac{pL}{2\pi} \right)^2 \right) \quad , \tag{25}$$

which is valid for momenta below the inelastic threshold. The regulated three-dimensional sum, $\mathbf{S}(x)$, is

$$\mathbf{S}\,(\,x\,) \;\equiv \lim^{\Lambda\to\infty} \left(\sum_{\mathbf{j}}^{|\mathbf{j}|<\Lambda} \frac{1}{|\mathbf{j}|^2 - x} \;-\; 4\pi\Lambda \right) \quad , \tag{26}$$

where the summation is over all triplets of integers $\mathbf{j}$ such that $|\mathbf{j}| < \Lambda$.

By performing an expansion in small $1/L$, the energy shift of n identical bosons in a finite volume, $\Delta E_n = E_n - nE_1$, has also been studied up to $\mathcal{O}(L^{-7})$ in recent work [32–35]. The resulting shift of energies due to both two-body and three-body interactions is given by [33]:

$$\begin{aligned}
\Delta E_n \;=\; & \frac{4\pi\, \overline{a}}{M\, L^3}\, {}^nC_2 \Bigg\{ 1 - \left(\frac{\overline{a}}{\pi\, L} \right) \mathcal{I} + \left(\frac{\overline{a}}{\pi\, L} \right)^2 \left[\mathcal{I}^2 + (2n-5)\mathcal{J} \right] \\
& - \left(\frac{\overline{a}}{\pi\, L} \right)^3 \left[\mathcal{I}^3 + (2n-7)\mathcal{I}\mathcal{J} + \left(5n^2 - 41n + 63 \right) \mathcal{K} \right] \\
& + \left(\frac{\overline{a}}{\pi\, L} \right)^4 \Big[\mathcal{I}^4 - 6\mathcal{I}^2\mathcal{J} + (4 + n - n^2)\mathcal{J}^2 + 4(27 - 15n + n^2)\mathcal{I}\,\mathcal{K} \\
& \qquad + (14n^3 - 227n^2 + 919n - 1043)\mathcal{L} \,\Big] \Bigg\} \\
& + {}^nC_3 \left[\frac{192\, \overline{a}^5}{M\pi^3 L^7} \left(\mathcal{T}_0 \;+\; \mathcal{T}_1\, n \right) \;+\; \frac{6\pi \overline{a}^3}{M^3 L^7}\, (n+3)\, \mathcal{I} \right] \\
& + {}^nC_3\, \frac{1}{L^6}\, \overline{\overline{\eta}}_3^{\,L} \quad + \; \mathcal{O}\left(L^{-8} \right) \quad ,
\end{aligned} \tag{27}$$

where ${}^mC_n = m!/(n!(m-n)!)$, and the parameter $\overline{a}$ is the inverse phase shift at the binding momentum of the two body system (below we will refer to this as the effective scattering length). This is related to the scattering length, a, and the effective range, r, by

$$a \;=\; \overline{a} \;-\; \frac{2\pi}{L^3} \overline{a}^3 r \left(\;1 \;-\; \left(\frac{\overline{a}}{\pi L} \right) \mathcal{I} \right) \quad . \tag{28}$$

The geometric constants entering Eq. (27) are:

$$\begin{aligned} \mathcal{I} &= -8.9136329\,, & \mathcal{J} &= 16.532316\,, & \mathcal{K} &= 8.4019240\,, \\ \mathcal{L} &= 6.9458079\,, & \mathcal{T}_0 &= -4116.2338\,, & \mathcal{T}_1 &= 450.6392\,. \end{aligned} \tag{29}$$

The three body parameter $\overline{\overline{\eta}}_3^L$ is constructed from the volume dependent but renormalization group invariant three body interaction parameter, $\overline{\eta}_3^L$, the inverse phase shift, $\overline{a}$, and the effective range, r, as

$$\overline{\overline{\eta}}_3^L \;=\; \overline{\eta}_3^L \left(\;1 \;-\; 6 \left(\frac{\overline{a}}{\pi L} \right) \mathcal{I} \right) \;+\; \frac{72\pi \overline{a}^4 r}{ML}\,\mathcal{I} \quad , \tag{30}$$

where

$$\overline{\eta}_3^L = \eta_3(\mu) \;+\; \frac{64\pi a^4}{M} \left(3\sqrt{3} - 4\pi \right) \log\left(\mu L\right) \;-\; \frac{96 a^4}{\pi^2 M} \mathcal{S}_{\rm MS} \quad . \tag{31}$$

and the renormalized scale dependent coupling $\eta_3(\mu)$ is responsible for the three-body interactions. The renormalization scheme dependent quantity $\mathcal{S}$ defined in the Minimal Subtraction scheme is given by $\mathcal{S}_{\rm MS} = -185.12506$.

A. Two-body interactions from Lüscher's method

From the energy difference in the 2-π^+ system, $\Delta E_{2\pi} = E_{2\pi} - 2m_\pi$, the relative momentum of each π^+, $\mathbf{p}$, in the center of mass frame (COM) can be calculated from the dispersion relation. We determine the effective scattering length[5], $\overline{a}$, by calculating the interacting momenta $\{\mathbf{p}_i\}$, on each bootstrap ensemble and applying Eq. (25), and we average over all ensembles to get the mean value of $\overline{a}$, and the statistical uncertainty. The systematic uncertainty is determined by averaging the systematic uncertainty of $\overline{a}$ on each ensemble resulting from the systematic uncertainty of the extracted energies from the choice of different fitting intervals. The extracted effective scattering length for each volume is shown in Table III. Our results are in agreement with the extractions in Ref. [36] from two-body systems studied on the same ensembles.

[5] As discussed above, $\bar{a}$ is the inverse phase shift at the binding momentum of the two body system, and the scattering length in Eq. (25) uses the Particle Physics sign convention, and it is negative for repulsive interactions.

TABLE III: The effective scattering length ($\overline{a}$) from Lüscher's method. The first uncertainty is statistical uncertainty and the second uncertainty is systematic.

$V^3 \times T$	p^2/m_π^2	$\overline{a}$(fm)	$m_\pi \overline{a}$
$16^3 \times 128$	0.0668(45)(1)	−0.134(7)(5)	0.263(15)(9)
$20^3 \times 256$	0.0301(9)(0)	−0.122(3)(1)	0.238(6)(1)
$24^3 \times 128$	0.0143(9)(1)	−0.106(6)(4)	0.203(12)(7)
$32^3 \times 256^a$	0.00678(54)(81)	−0.114(9)(13)	0.223(17)(26)

[a]Results for this ensemble are taken from Ref. [36].

TABLE IV: The effective scattering length ($\overline{a}$) and $m_\pi f_\pi^4 \overline{\overline{\eta}}_3^L$ extracted from fits to different ranges of n. For a fixed $n_{\max}$, the χ^2/d.o.f. is larger in smaller volumes, indicating that Eq. (27) fails to describe systems of high densities.

	$n = [3, 5]$			$n = [3, 6]$		
$V^3 \times T$	$m_\pi \overline{a}$	$m_\pi f_\pi^4 \overline{\overline{\eta}}_3^L$	χ^2/dof	$m\overline{a}$	$m_\pi f_\pi^4 \overline{\overline{\eta}}_3^L$	χ^2/dof
$16^3 \times 128$	0.260(14)(2)	0.70(10)(4)	1.0	0.261(14)(1)	0.67(9)(3)	1.5
$20^3 \times 256$	0.234(6)(1)	0.80(8)(3)	0.25	0.235(6)(1)	0.79(7)(1)	0.5
$24^3 \times 128$	0.209(11)(4)	1.61(20)(20)	0.26	0.209(11)(3)	1.59(18)(12)	0.25
	$n = [3, 7]$			$n = [3, 8]$		
$V^3 \times T$	$m_\pi \overline{a}$	$m_\pi f_\pi^4 \overline{\overline{\eta}}_3^L$	χ^2/dof	$m_\pi \overline{a}$	$m_\pi f_\pi^4 \overline{\overline{\eta}}_3^L$	χ^2/dof
$16^3 \times 128$	0.262(14)(1)	0.64(9)(1)	3.5	0.263(14)(1)	0.62(8)(1)	5.5
$20^3 \times 256$	0.235(6)(5)	0.79(7)(1)	1.1	0.235(6)(1)	0.76(7)(1)	2.8
$24^3 \times 128$	0.211(11)(2)	1.56(17)(8)	0.4	0.210(11)(2)	1.50(16)(5)	1.0

B. Interaction parameters from small $\overline{a}/L$ expansion

The dimensionless qualities $m_\pi \overline{a}$ and $m_\pi f_\pi^4 \overline{\overline{\eta}}_3^L$ can be extracted by fitting ΔE_n to the large volume expansion of Eq. (27). The fitting strategy is similar to that used in Lüscher's method by first fitting to each bootstrap ensemble and then computing the distribution of fitted parameters in order to get statistical and systematic uncertainties. There are two ways to extract $m\overline{a}$. One is by fitting only to ΔE_2 using Eq. (27) with the last two lines set to zero, and the other way is by fitting multiple ΔE_n's, with $n \geq 3$, and extracting $m_\pi f_\pi^4 \overline{\overline{\eta}}_3^L$ at

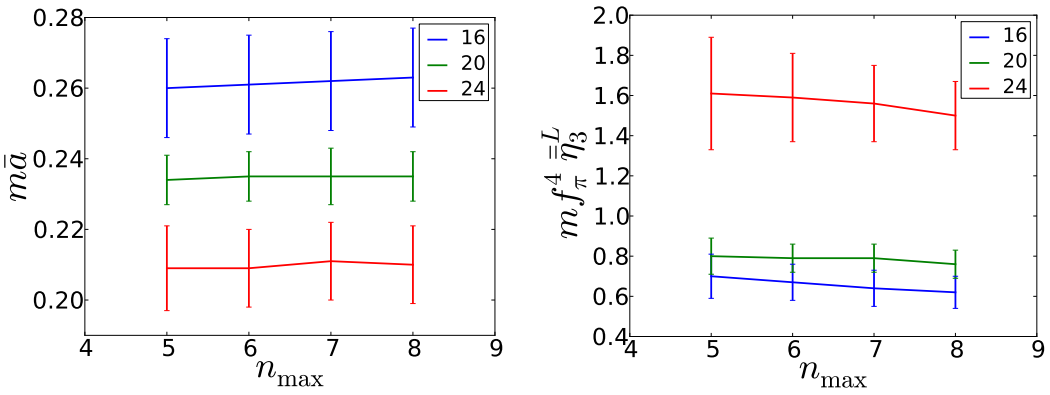

FIG. 15: The $m\overline{a}$ and $mf_\pi^4\overline{\overline{\eta}}_3^L$ extracted from different fitting windows $[n_{\min}, n_{\max}]$ with $n_{\min} = 3$ fixed and varying $n_{\max}$.

the same time as is shown in Table. IV and Fig. 15. The final $\overline{a}$ and $mf_\pi^4\overline{\overline{\eta}}_3^L$ extracted from the later method are chosen from fits with $\chi^2 \sim 1$. We are forced to to use only few body systems as the quality of fit rapidly decreases for large numbers of pions. This suggests that the weakly interacting pion model of the system that Eq. (27) encodes is becoming less valid. Results for the two-body interaction extracted in both ways agree within uncertainties with those extracted using Lüscher's method, and are shown in Table V. The original data for the ΔE_n's and the results from the fits are shown in Fig. 16.

TABLE V: The effective scattering length ($\overline{a}$) from small $\overline{a}/L$ expansion. The symbol "[2]" indicates that only ΔE_2 is used in the fitting, and "[3,6]" means that all ΔE_3 to ΔE_6 are used.

$V^3 \times T$	$m_\pi\overline{a}$[2]	$m_\pi\overline{a}$[3, 6]	$k\cot\delta/m_\pi$	$m_\pi f_\pi^4\overline{\overline{\eta}}_3^L$[3,6]
$16^3 \times 128$	0.259(14)(5)	0.260(14)(2)	−3.85(21)(3)	0.70(10)(4)
$20^3 \times 256$	0.234(6)(1)	0.235(6)(5)	−4.26(11)(10)	0.79(7)(1)
$24^3 \times 128$	0.205(12)(5)	0.210(11)(2)	−4.78(25)(7)	1.50(16)(15)

The effective scattering length, $\overline{a}$, extracted from the three volumes depend on the volume. With multiple volumes, Eq. (27) can be inverted to extract both the scattering length, a, and the effective range, r. During the fit, we have also used $k\cot\delta/m_\pi$ determined on a matching $32^3 \times 256$ and $24^3 \times 128$ ensembles from Ref. [36] with all lattice parameters the same. We are using the simplest form, $k\cot\delta/m_\pi = -\frac{1}{m_\pi a} + \frac{m_\pi r}{2}(\frac{k^2}{m_\pi^2})$, and neglecting higher order shape parameters as our interacting momenta are small. The infinite volume results

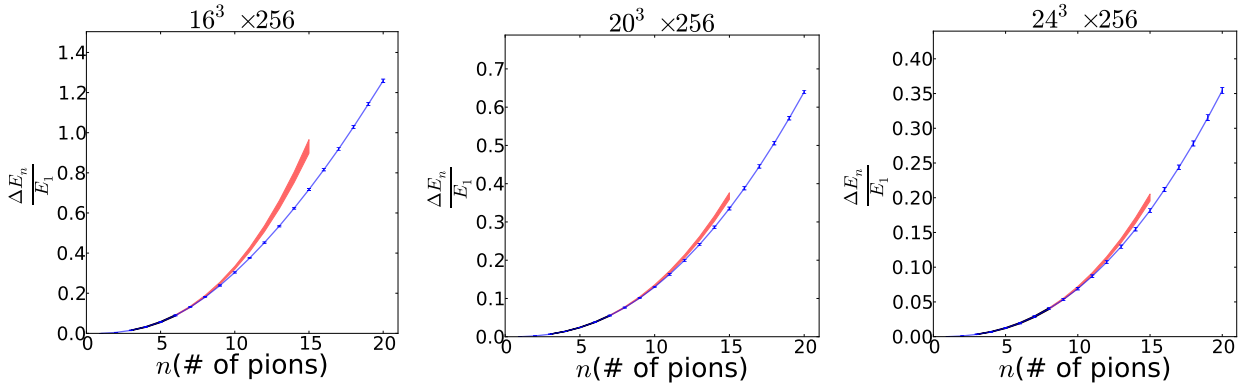

FIG. 16: The energy differences, ΔE_n, are plot as a function of the number of pions, n, where the blue points are the original data, the red bands are the fits, and the black bands are the regions where the fits are performed. From the left to right, ΔE_n from 16^3, 20^3, 24^3 are shown.

are $1/m_\pi a = 4.73(15)(13)$ and $m_\pi r = 27.4(7.9)(4.7)$, which agree with the determinations of Ref. [36]. The first error is the statistical error, and the difference between the infinite volume results by fitting with the data from the two ensembles in Ref. [36] and without them is taken as an additional systematic error. Both fits are shown in Fig. 17.

By utilizing the extracted effective range, r, and the effective scattering length, $\overline{a}(L)$, from the three different volumes, from Eq. (30), the volume dependent parameter $\overline{\eta}_3^L$, responsible for the three-body interactions can be determined for each volume. The extracted values of $\overline{\eta}_3^L$ are shown in Fig. 18. The dependence of $\overline{\eta}_3$ on the volume can be rewritten from Eq. (31) into a simpler form

$$\overline{\eta}_3^L(L) = C + \frac{\alpha a^4}{M}\log(L), \tag{32}$$

where C contains contributions independent of L, and $\alpha = 64\pi(3\sqrt{3} - 4\pi) = -1.48 \times 10^3$. We fit $\overline{\eta}_3^L$ to our data to determine C and the best fit is shown in Fig. 18. However the χ^2 of the fit is poor and it appears that Eq (32) does not effectively explain the volume dependence of our data. This might come from the competing of higher order terms $\mathcal{O}(\frac{1}{L^3})$, but it also may be a statistical effect. The large value of $\overline{\eta}_3^L$ for $L = 24$ is correlated with a down shift of the scattering length $\overline{a}$. In Ref. [36], a value of $m\overline{a} = 0.236(18)(27)$ was found for $L = 24$, which agrees with the value $m\overline{a} = 0.210(16)(5)$ found above, but with a larger central value, perhaps indicating a statistical fluctuation.

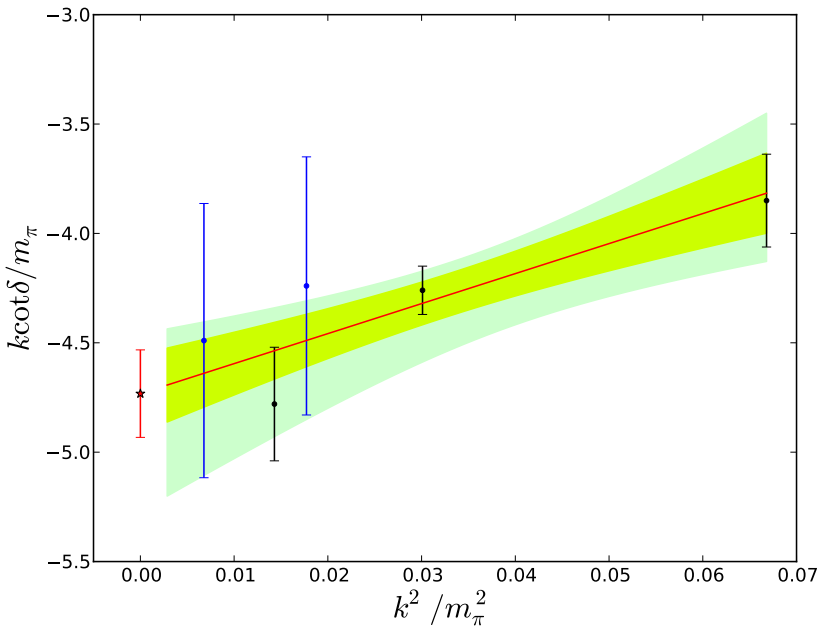

FIG. 17: The scattering phase shifts from 16^3, 20^3, and 24^3 ensembles in this study, are shown as the black data points from right to left respectively. The blue data points are the 24^3 and 32^3 ensemble results from Ref. [36] from right to left respectively. The inner shaded region is the fit to all data, and the outer shaded region is the fit only to the data in this paper, and the star is the infinite volume result.

VI. QCD PHASE DIAGRAM AT NON-ZERO μ_I

In Fig. 19, we show the energy density, $\epsilon = \frac{E}{V}$, determined from the ground state energies, $E_{n\pi}$ that have been computed on each of the three volumes. For a fixed n, the pions are forced to be closer to each other in a smaller volume, and the repulsive interactions between them become stronger. This drives up the energy of the whole system. The energy densities are weakly dependent on the volume, however there are slightly differences as shown in the inset of Fig. 19.

From the extracted ground state energies, the isospin chemical potential can also be determined by a backward finite difference, $\mu_I\,(n) = \frac{dE}{dn} \sim E_n - E_{n-1}$. We calculate $\mu_I(n)$ on each bootstrap ensemble, which accommodates correlations between $E_{n\pi}$'s extracted on the same ensemble, and the systematic uncertainty of the $\mu_I(n)$ from each ensemble is evaluated by adding systematic uncertainty from varying the fit ranges used to determine

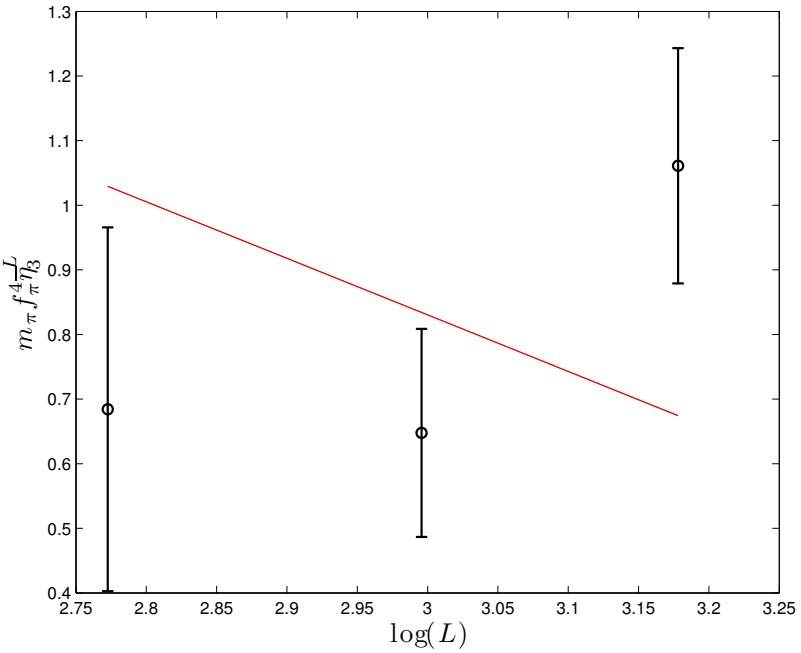

FIG. 18: The extracted three-body interaction parameter, $\overline{\eta}_3^L(L)$, is plotted as a function of the spatial extent of the lattice, L, (black points). The red line shows the expected dependence of $\overline{\eta}_3^L$ on L from Eq. (32) with $C = 4.3$, which clearly does not provide a good description of the data.

E_n and E_{n-1} in quadrature. The final systematic uncertainty on $\mu_I(n)$ is from averaging the systematic uncertainties of all the bootstrap ensembles, and the statistical uncertainty is the standard deviation of the values of $\mu_I(n)$ on the individual bootstrap ensembles.

In Fig. 20, the dependence of $\mu_I/m_\pi - 1$ on the isospin density ρ_I is shown for the three volumes. The isospin chemical potential exhibits similar behaviour in all three volumes, where they overlap. At small ρ_I, μ_I increases at an accelerating rate, in agreement with the prediction from chiral perturbation theory (χPT) [8], however at around $\rho_I \approx 0.5$ fm^{-3} the behaviour of μ_I starts to change, and the accelerating rate gradually decreases, and at even higher isospin density the μ_I starts to flatten off. This change of behaviour of μ_I indicates that the physical state of the system may be altering.

The expected phase structure of QCD at non-zero isospin chemical potential has been discussed in Ref. [8]. At zero temperature, when $\mu_I < m_\pi$, there is not enough energy to excite a pion out of the vacuum. As soon as μ_I reaches m_π, pions can be produced and the system enters a phase with a pion condensate (BEC) via a second order phase transition.

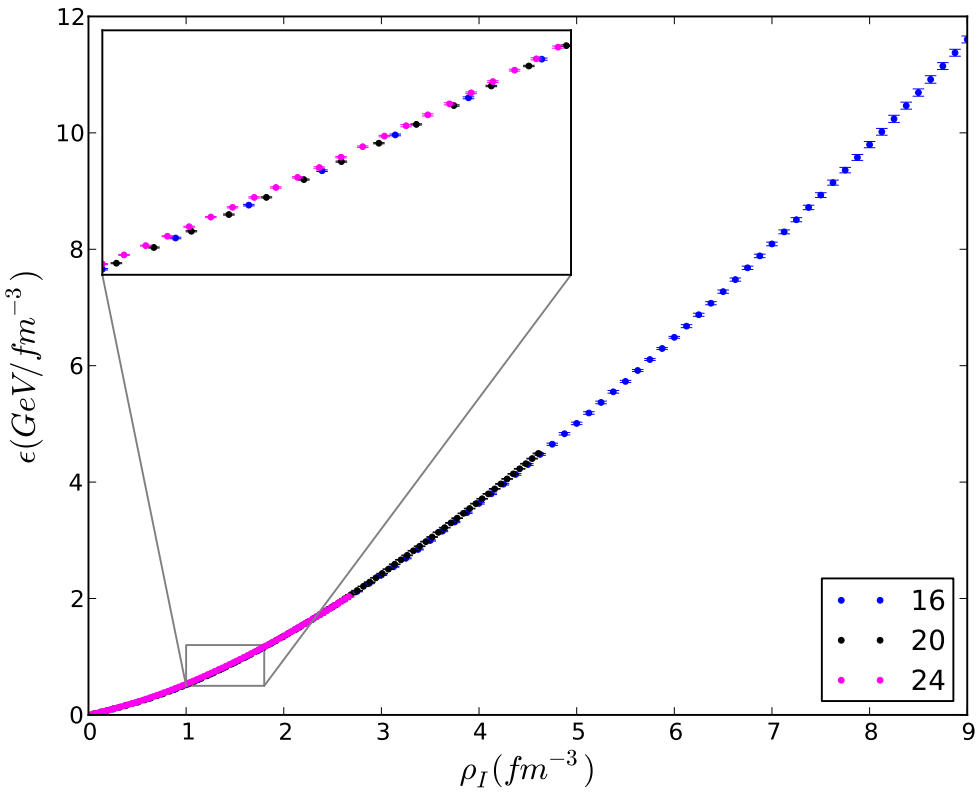

FIG. 19: Energy densities (ϵ) calculated on 3 different volumes are shown as a function of isospin density. The blue points are from the 16^3 ensemble, the black ones are from the 20^3 ensemble and the pink one are from the 24^3 ensemble. The inset show the slight difference in energy density on three ensembles.

At asymptotically large values of μ_I, the attractive nature of one gluon exchange guarantees the existence of a BCS-like state in which quark–anti-quark Cooper pairs are formed. At an intermediate value of μ_I a BEC-BCS crossover is conjectured [8].

In this paper, our calculations are performed at a small but nonzero temperature, $\mathcal{T} \sim 20$ MeV. With the canonical method used in the current calculation, the lowest isospin chemical potential that we probe is $\mu_I = m_\pi$ by definition as we directly add π^+'s into the system. In the smallest volume, for $n = 72$ π^+'s (the largest value we consider), an isospin density of $\rho_I \sim 9$ fm^{-3} is achieved, and the phase diagram is explored from $\mu_I = m_\pi$ up to $\mu_I \approx 4.5\, m_\pi$ in this paper as shown by the red dashed line in Fig. 21.

In order to investigate the possible phase transition suggested by the behaviour of the isospin chemical potential in more detail, we have also compared the extracted energy density

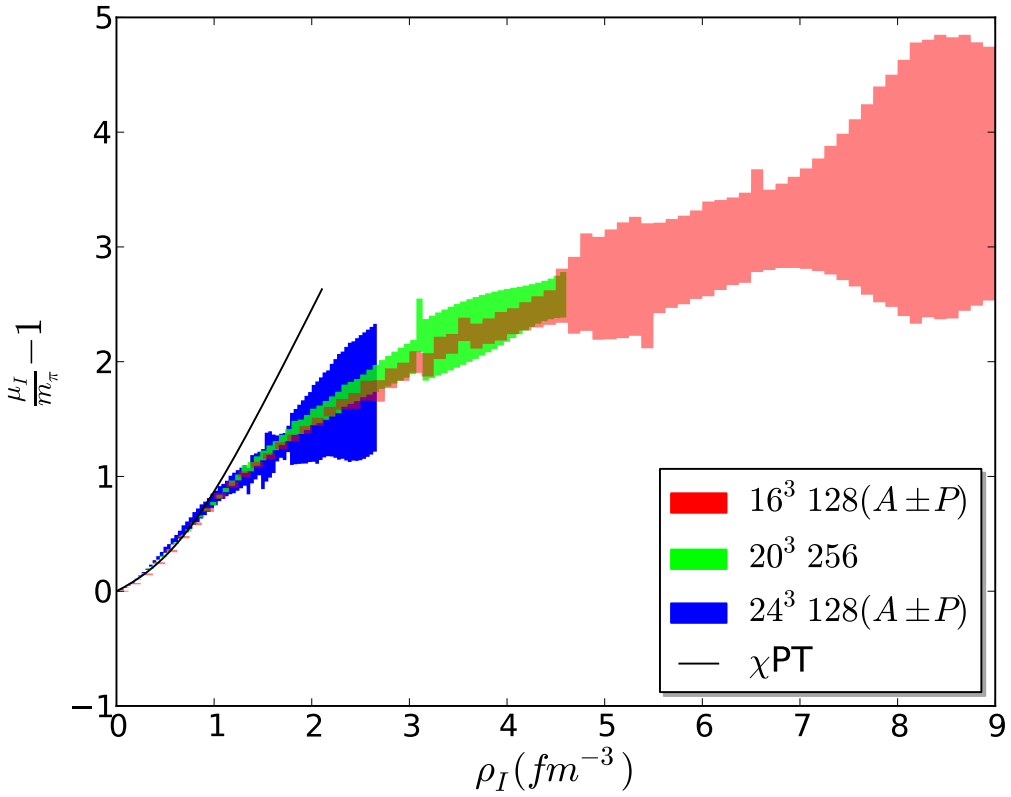

FIG. 20: The isospin chemical potential, μ_I, is plotted as a function of the isospin density, ρ_I, from three lattice ensembles, B1 (red), B3 (blue) and B4 (green). The solid black line is from expectations of χPT [8]

with the energy density of a cold degenerate system described by a model of weakly interacting quarks filling their Fermi sphere up to a maximum momentum $k_F \approx E_F = \mu_I$ [37]. This Stefan-Boltzmann energy density is given by

$$\epsilon_{SB} = \frac{N_f N_c}{4\pi^2}\mu_I^4 \tag{33}$$

where $N_f = 3$ and $N_c = 3$. The ratio of ϵ/ϵ_{SB} is plotted in Fig. 22, and exhibits similar behaviours in all three volumes. The ratio increases from $\mu_I = m_\pi$ to a peak around $\mu_I \approx 1.3\ m_\pi$, and then drops and eventually begins to plateau at around $\mu_I \approx 3\ m_\pi$. Peak positions, μ^I_{peak}, for each volume identified from Fig. 22 are $\mu^I_{peak} = \{1.20(5), 1.25(5), 1.27(5)\}\ m_\pi$ for $L = \{16, 20, 24\}$ respectively. With an extrapolation linear in $1/L^3$, the peak position in infinite volume is $\mu^I_{peak} = 1.30(7)\ m_\pi$. The system for $\mu_I < 1.3\ m_\pi$, can be identified as a pion gas. When $\mu_I \sim \mu^I_{peak}$, pions start to condense and the system resides in the BEC

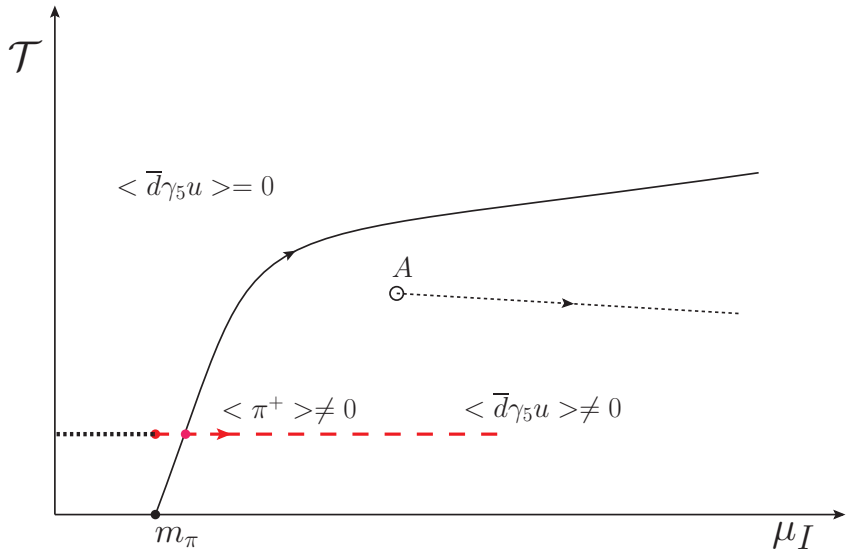

FIG. 21: Expected QCD phase diagram following Ref. [8]. Our calculations at a fixed temperature, $\mathcal{T} \sim 20$ MeV probe the phase structure along the red dashed line from $\mu_I = m_\pi$ to $\mu_I = 4.5\ m_\pi$.

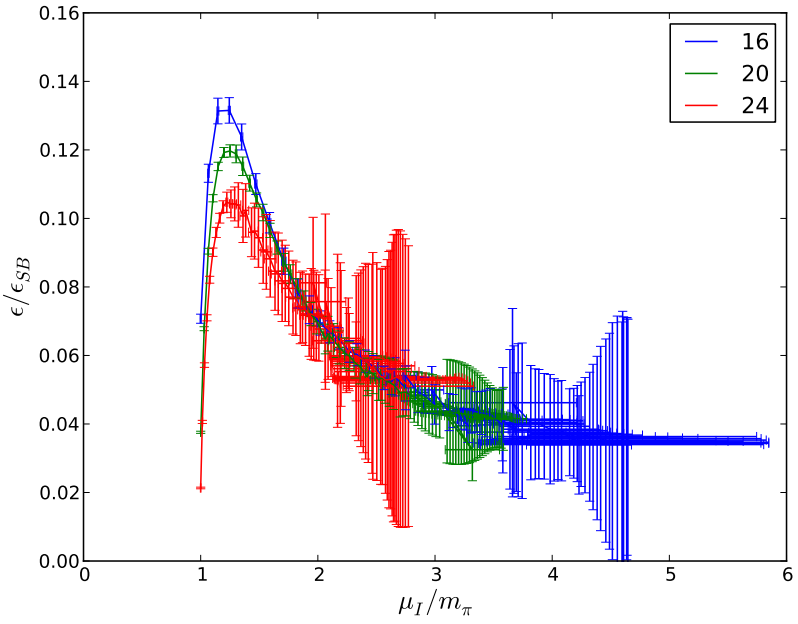

FIG. 22: The ϵ/ϵ_{SB} is plotted as a function of μ_I/m_π.

state. The plateau beginning to form beyond $\mu_I \approx 3\ m_\pi$, may indicate a crossover from the BEC to BCS state, however higher precision and larger μ_I is required to make a definite statement. Discretization effects also remain to be investigated.

Two flavour QCD with finite μ_I at large $\mathcal{T}$ has been investigated in Ref. [12], where a finite temperature deconfinement phase transition was identified at $\mu_I < m_\pi$, however for $\mu_I > m_\pi$ no results were presented. In Ref. [14], the phase diagram of $N_f = 4 + 4$ QCD was investigated at different temperatures and values μ_I using the grand canonical approach, and a phase transition from a pion gas to a BEC state has also been suggested at μ_I slightly higher than m_π, in agreement with the results found here. Two color QCD has been studied in Ref. [37], where the authors identified the transition from vacuum to BEC state and the BEC/BCS transition. Somewhat interestingly, the ratio of the energy density and its Stefan-Boltzmann limit has also been studied (inset of Fig. 1 in Ref. [37]), showing qualitatively similar behaviour to that found in the current study.

VII. CONCLUSION

In this work, we have studied lattice QCD at non-zero isospin chemical potential using a canonical approach in which we have investigated systems with the quantum numbers of up to 72 π^+'s in three lattice volumes, $L^3 \sim (2.0, 2.5 \text{ and } 3.0 \text{ fm})^3$ at a pion mass of $m_\pi \sim 390$ MeV at a single lattice spacing. In order to perform this study, we have developed several new methods for performing the requisite Wick contractions of quark field operators. These methods are an enormous computational improvement over previous approaches and their accuracy and performance have been carefully investigated.

In our analysis, we have determined the ground state energies of multi-pion systems in three different volumes and have used this to extract the isospin chemical potential of the states that are produced. In the smallest volumes, systems with isospin chemical potentials of up to $\mu_I \sim 1600$ MeV are created. By considering the energy density as a function of the isospin chemical potential, we provide strong evidence for the transition of the system from a weakly interacting pion gas to a Bose-Einstein condensed (BEC) phase at $\mu \sim m_\pi$ as expected from χPT. At higher values of the chemical potential the system is expected to transition to a BCS state and we have sought numerical evidence for this but do not have conclusive results. It is interesting to note that the behaviour of the energy density as a function of the isospin chemical potential is very similar to that recently found in two-colour QCD with a baryon chemical potential by Hands et al. [37].

By focusing on few pion systems, we have extracted the two and three pion interactions,

determining the scattering length, effective range and the renormalisation group invariant effective three-body interaction. The scattering parameters were found to be in good agreement with other recent determinations and we have attempted to investigate the intrinsic volume dependence of the renormalisation group invariant three-pion interaction. We have also found that as the density increases and the system transitions to a BEC, it can no longer be well described in terms of weak few-body interactions.

VIII. ACKNOWLEDGEMENT

We thank Josh Erlich, Martin Savage and Masanori Hanada for valuable discussions. We appreciate the support of the DOE NERSC facility, NSF XSEDE resources and in particular TG-PHY080039N, as well as the Sporades cluster at the College of William & Mary. The work of WD, KO and ZS was supported in part by JSA, LLC under DOE contract No. DE-AC05-06OR-23177 and by the Jeffress Memorial Trust, J-968. WD and KO were supported in part by DOE grant DE-FG02-04ER41302. WD was also supported by DOE OJI Award DE-SC000-1784.

---

[1] S. R. Beane *et al.* [NPLQCD], Phys. Rev. D **80**, 074501 (2009) [arXiv:0905.0466].

[2] T. Yamazaki, Y. Kuramashi, and A. Ukawa, Phys. Rev. D **81**, 111504 (2010) [arXiv:0912.1383].

[3] S. R. Beane, W. Detmold, T. C. Luu, K. Orginos, M. J. Savage and A. Torok, Phys. Rev. Lett. **100**, 082004 (2008) [arXiv:0710.1827].

[4] W. Detmold, M. J. Savage, A. Torok, S. R. Beane, T. C. Luu, K. Orginos and A. Parreño, Phys. Rev. D **78**, 014507 (2008) [arXiv:0803.2728].

[5] W. Detmold, K. Orginos, M. J. Savage and A. Walker-Loud, Phys. Rev. D **78**, 054514 (2008) [arXiv:0807.1856].

[6] W. Detmold, B. Smigielski Phys. Rev. D **84**, 014508 (2011) [arXiv:1103.4362].

[7] D. B. Kaplan, A. E. Nelson Phys. Lett. **B175**,57 (1986).

[8] D. T. Son and M. A. Stephanov Phys. Rev. Lett. **86**, 592 (2001) [arxiv:hep-lat/0005225].

[9] M. Hanada, N. Yamamoto [arXiv:1103.5480].

[10] M. Hanada, C. Hoyos, A. Karch, L. G. Yaffe [arXiv:1201.3718].

[11] M. Hanada, Y. Matsuo, N. Yamamoto [arXiv:1205.1030].

[12] J. B. Kogut and D. K. Sinclair, Phys. Rev. D **70**, 094501 (2004) [arXiv:hep-lat/0407027].

[13] D. K. Sinclair and J. B. Kogut, PoS **LAT2006**, 147 (2006) [arXiv:hep-lat/0609041].

[14] Ph. de Forcrand, M. A. Stephanov, U. Wenger PoS **LAT2007**, 237 (2007) [arXiv:hep-lat/0711.0023].

[15] W. Detmold and M. J. Savage, Phys. Rev. D**82**, 014511 (2010) [arxiv:1001.2768].

[16] Z. Shi, W. Detmold, PoS **LAT 2011**, 328 (2011) [arXiv:1111.1656].

[17] H. W. Lin, S. D. Cohen, J. Dudek, R. G. Edwards, B. Joó, D. G. Richards, J. Bulava, J. Foley, C. Morningstar, E. Engelson, S. Wallace, K. J. Juge, N. Mathur, M. J. Peardon, S. M. Ryan, Phys. Rev. D **79**, 034502 (2009) [arXiv:0810.3588].

[18] N. Macon, A. Spitzbart, The American Mathematical Monthly, Vol. **65**, No. 2: 95100 (1958).

[19] D. H. Bailey, Y. Hida, X. S. Li, B. Thompson, "ARPREC: An arbitrary precision computation package," September 2002. Available at http://crd.lbl.gov/∼dhbailey/dhbpapers/arprec.pdf.

[20] Y. Hida, X. S. Li, and D. H. Bailey. "Quad-double arithmetic: Algo- rithms, implementation, and application." Technical Report LBNL-46996, (2000).

[21] B. Sheikholeslami, R. Wohlert, Nucl. Phys. B**259**, 572 (1985).

[22] M. Okamoto *et al.* [CP-PACS Collaboration], Phys. Rev. D **65**, 094508 (2002) [arXiv:hep-lat/0112020].

[23] P. Chen, Phys. Rev. D **64**, 034509 (2001) [arXiv:hep-lat/0006019].

[24] B. Sheikholeslami, R. Wohlert, Nucl. Phys. B**259**, 572 (1985).

[25] C. Morningstar, M. Peardon, Phys. Rev. D**69**, 054501 (2004) [arXiv:hep-lat/0311018].

[26] T. Blum, P. Chen, N. Christ, C. Cristian, C. Dawson, G. Fleming, R. Mawhinney, S. Ohta, G. Siegert, A. Soni, P. Vranas, M. Wingate, L. Wu, Y. Zhestkov, Phys. Rev. D **68**, 114506 (2003) [arXiv:hep-lat/0110075].

[27] Y. Aoki, T. Blum, N. H. Christ, C. Dawson, T. Izubuchi, R. D. Mawhinney, J. Noaki, S. Ohta, K. Orginos, A. Soni, N. Yamada, Phys. Rev. D **73**, 094507 (2006) [arXiv:hep-lat/0508011].

[28] C. Aubin, J. Laiho, R. S. Van de Water, Phys. Rev. D **81**, 014507 (2010) [arXiv:0905.3947].

[29] M. Lüscher, Commun. Math. Phys. **105**, 153 (1986).

[30] M. Lüscher, Nucl. Phys. B **354**, 531 (1991).

[31] S. R. Beane, P. F. Bedaque, A. Parreño and M. J. Savage, Phys. Lett. B **585**, 106 (2004) [arXiv:hep-lat/0312004].

[32] S. R. Beane, W. Detmold and M. J. Savage, Phys. Rev. D **76**, 074507 (2007) [arXiv:0707.1670].

[33] W. Detmold and M. J. Savage, Phys. Rev. D **77**, 057502 (2008) [arXiv:0801.0763].

[34] S. Tan, Phys. Rev. A **78**, 013636 (2008) [arXiv:0709.2530].

[35] B. Smigielski and J. Wasem Phys. Rev. D **79**, 054506 (2009) [arXiv:0811.4392].

[36] S. R. Beane, E. Chang, W. Detmold, H. W. Lin, T. C. Luu, K. Orginos, A. Parreño, M. J. Savage, A. Torok, A. Walker-Loud, Phys. Rev. D **85**, 034505 (2012) [arXiv:1107.5023].

[37] S. Hands, S. Kim, J. I. Skullerud, Phys. Rev. D**81**, 091502 (2010) [arXiv:1001.1682].